Chemical Physics Reviews

REVIEW ARTICLE | APRIL 21 2026

Charge carrier extrinsic energy filtering: Theoretical advances, applications, and perspectives in thermoelectricity

A. Mazzacua ; F. Giulio ; D. Narducci

Check for updates

Chem. Phys. Rev. 7, 021302 (2026)
https://doi.org/10.1063/5.0260985

View Online
Export Citation

Articles You May Be Interested In

Synthesis of thermoelectric bismuth telluride alloys by sol-gel auto-combustion method

AIP Conf. Proc. (August 2023)

Enhancement of thermoelectric power factor in $CaGe_2$ films through interlayer atomic modulation

Appl. Phys. Lett. (March 2025)

Thermoelectricity

Physics Today (February 1959)

05 May 2026 08:18:17

AIP Publishing

Special Topics Open for Submissions

Learn More

AIP Publishing

Chemical Physics Reviews REVIEW pubs.aip.org/aip/cpr

Charge carrier extrinsic energy filtering: Theoretical advances, applications, and perspectives in thermoelectricity

Cite as: Chem. Phys. Rev. **7**, 021302 (2026); doi: 10.1063/5.0260985
Submitted: 28 November 2025 · Accepted: 7 April 2026 ·
Published Online: 21 April 2026

View Online Export Citation CrossMark

A. Mazzacua,[a] F. Giulio,[b] and D. Narducci[c]

AFFILIATIONS

University of Milano Bicocca, Department of Materials Science, via R. Cozzi 55, 20125 Milan, Italy

[a]Electronic mail: a.mazzacua@campus.unimib.it
[b]Electronic mail: federico.giulio@unimib.it
[c]Author to whom correspondence should be addressed: dario.narducci@unimib.it

ABSTRACT

Extrinsic energy filtering (EEF) selectively allows high-energy charge carriers to pass through an energy barrier, blocking lower-energy (cold) carriers. This mechanism enhances thermoelectric performance by increasing the Seebeck coefficient S, since only high-energy carriers contribute, while maintaining electrical conductivity σ due to their higher mobility despite lower carrier density. The combined effect significantly boosts the power factor (PF) σS^2. The concept of EEF dates back nearly 50 years, initially demonstrated by embedding metallic nanoparticles in telluride materials. Since then, theoretical models have advanced, and practical implementations have expanded to include elemental semiconductors, chalcogenides, and recently polymers. Nanostructured systems have played a key role by enabling close comparisons between theory, computational simulations, and experiments, deepening the understanding of EEF physics. This review offers a critical overview of both theoretical foundations and experimental progress in EEF over five decades. It highlights criteria for identifying genuine energy filtering effects in real materials and stresses the importance of distinguishing this phenomenon from other mechanisms that also improve the thermoelectric PF.

© 2026 Author(s). All article content, except where otherwise noted, is licensed under a Creative Commons Attribution (CC BY) license (https://creativecommons.org/licenses/by/4.0/). https://doi.org/10.1063/5.0260985

TABLE OF CONTENTS

I. INTRODUCTION

In the search for alternate energy sources, any policy mitigating power waste has a pivotal place, considering that more than 50% of energy is currently wasted as discarded heat. Along with improving engine and process efficiency, recovering low-enthalpy heat provides a significant instrument. Additionally, heat may serve as a ubiquitous power source for low-power distributed devices.[1] Thermoelectricity actually meets both aims, qualifying as a key technology toward a sustainable development.

The conversion efficiency of a thermoelectric material is related to its dimensionless figure of merit $zT = S^2\sigma T/\kappa$, where S is the

05 May 2026 08:18:17

© Author(s) 2026

Seebeck coefficient, σ is the electrical conductivity, κ is the total thermal conductivity (the sum of electronic and lattice contribution $\kappa_e + \kappa_{lat}$), and T is the absolute temperature. Much effort has been made during the last few years to enhance the thermoelectric performance of different materials. The most important limitation to increase zT is the mutual dependence of S, σ, and κ. Good electrical conductors are also good thermal conductors while σ and S show opposite dependency on carrier density, with σ increasing and S decreasing when the carrier density increases.[2] Nonetheless, over the years the thermoelectric community has pursued strategies to enhance zT by decoupling S, σ, and κ, mostly by taking advantage of nanotechnologies.[3] To decrease the thermal conductivity while retaining large electrical conductivities, size effects taking advantage of the difference between the phonon and the electronic mean-free path (mfp) allowed for remarkable enhancements of zT in silicon.[4,5] Concerning instead the power factor PF$= \sigma S^2$, several routes have been considered after the 1993 visionary papers by Hicks and Dresselhaus.[6,7] They include nanostructuring bulk materials,[8] band engineering and modulation doping,[9] energy filtering (EF),[10] quantum-confinement,[11] and resonant states (RSs).[12] This review will focus on energy filtering (EF), which is proving not only as an effective strategy in several materials but has also the remarkable advantage of being deployable both in thin film and bulk materials, both through bottom-up and top-down preparation strategies.

By energy filtering, we will strictly refer to a mechanism of energy-dependent charge carrier scattering. It may be implemented in two different ways. In *extrinsic* energy filtering (EEF), the filtering process is carried out by potential barriers which are able to stop low-energy carriers (cold carriers) without obstructing the high-energy carriers (hot carriers). Thus, EEF leads to an increase in S, as the carrier density is reduced. At the same time, the lower carrier density is counterbalanced by the larger mobility μ of hot (mobile) carriers, mitigating and sometimes even increasing σ with respect to the unfiltered case. Along a different avenue, theoretical and experimental evidence has been put forward about the possibility of filtering carriers by directly controlling the carrier relaxation time $\tau(E)$, overlapping flat and dispersive bands around the Fermi level. As a result, charge carriers undergo energy-dependent interband scattering through a mechanism named *intrinsic* energy filtering (IEF).[13]

This paper is organized as follows: Sec. II will provide an introduction to the concept of energy filtering, both intrinsic and extrinsic. Extrinsic energy filtering will be then discussed in greater details in Sec. III, also reviewing the historical evolution of the concept. Based on such modeling, Sec. IV will suggest criteria that experimentalists might like to consider to properly identify EEF in real materials. Applications of such criteria to thermoelectric materials will be the subject of Sec. V.

II. PHYSICAL PRINCIPLES OF ENERGY FILTERING

A. Engineering carrier relaxation time

Basics of energy filtering find a simple explanation by solving the Boltzmann transport equation (BTE) under the relaxation time approximation.[14] The Seebeck coefficient and electrical conductivity compute, as known, to

$$S = \frac{1}{qT}\frac{\int_0^\infty E\tau(E)(E-E_f)g(E)\frac{\partial f_0}{\partial E}dE}{\int_0^\infty E\tau(E)g(E)\frac{\partial f_0}{\partial E}d(E)}, \tag{1}$$

where $g(E)$ is the density of states, f_0 is the Fermi–Dirac distribution, $\tau(E)$ is the carrier energy-dependent relaxation time, E_f is the Fermi energy, T is the absolute temperature, and q is the carrier charge; and

$$\sigma = -\frac{2q^2}{3m^*}\int_0^\infty E\tau(E)g(E)\frac{\partial f_0}{\partial E}d(E), \tag{2}$$

where m^* is the carrier effective mass. Defining a spectral electrical conductivity $\sigma(E)$ as

$$\sigma(E) = -\frac{2q^2}{3m^*}E\tau(E)g(E)\frac{\partial f_0}{\partial E}, \tag{3}$$

one can rewrite S as

$$S = -\frac{3m^*}{2q^3T}\langle E - E_f\rangle_\sigma, \tag{4}$$

where the average $\langle\cdots\rangle_\sigma$ is computed using $\sigma(E)$ as the weight factor. Since $\frac{\partial f_0}{\partial E}$ is significantly different from zero only in a narrow window around E_f, expanding Eq. (3) around E_f one obtains[14]

$$\sigma(E) = -\frac{2q^2}{3m^*}\left(E\tau(E_f)g(E_f) + E_f\frac{\mathrm{d}(\tau(E)g(E))}{\mathrm{d}E}\bigg|_{E=E_f}\delta E\right). \tag{5}$$

Equation (5) shows how the shape of $g(E)\tau(E)$ around E_f rules S and σ. In *most* metals and metallic alloys, high σ values are due to large yet flat $g(E)$ around E_f, leading in turn to low S. Instead, semiconductors show asymmetric $g(E)$ around E_f, leading to high S values, with σ still being ruled by $g(E)$. This also anticipates how the asymmetry of $g(E)\tau(E)$ may be used to achieve increases of S and σ.

B. Extrinsic energy filtering

With EEF, energy-dependent carrier scattering rate stems from compositional inhomogeneities in a material, leading to the generation of potential barriers. Typical examples are precipitates at grain boundaries (GBs) or within the material's matrix and top-down phase boundaries in layered nanostructures. In polycrystalline phases, the potential barriers at GBs are well known to cause carrier scattering, simply reducing carrier mobility.[15] This is the case since the potential barrier usually largely exceeds k_BT (where k_B is the Boltzmann's constant), letting carriers to flow through the phase only upon thermionic emission or, when the barrier width is very small, by tunneling. However, when the barrier height E_b is comparable to k_BT, carriers undergo energy filtering. Only hot carriers, with energies exceeding E_b, move throughout the system, overcoming the barriers. Therefore, in n (p) type semiconductors the electron (hole) relaxation time display a sharp change at $E = E_{cb} + E_b$ ($E = E_{vb} - E_b$), where E_{cb} (E_{vb}) is the conduction (valence) band edge energy. However, filtering in itself is not sufficient to make EEF of use to enhance the thermoelectric power factor (PF). The reduction of mobile charge carriers is cause of an increase in $|S|$. Yet, it would also cause a decrease in the electrical conductivity, not necessarily counterbalancing the increase in the Seebeck coefficient. However, since the carrier spectral mobility $\mu(E)$ scales with $\tau(E)$ as $\mu(E) = (q/m^*)\tau(E)$, then, *when no other mechanism substantially limit carrier mobility*, the decreased mobile

05 May 2026 08:18:17

© Author(s) 2026

carrier density may be compensated (and sometimes even overcompensated) by the increase in its average value $\bar{\mu}$. As will be shown, this implies that carrier drift and diffusion must occur (semi)ballistically across the interbarrier region. Additionally, precipitates and GBs also reduce the thermal conductivity. This will be shown (cf. Sec. V) to contribute to enhance the material's zT.

The absence of additional scattering mechanisms is rarely met in real systems. Impurity scattering (both from neutral and ionized centers) along with electron–phonon scattering are ubiquitous in doped semiconductors at room temperature and above. It should be noted, however, that they decrease relaxation times (and mobility thereof) also in the absence of EEF. Therefore, their impact on mobile (hot) carriers when EEF is activated is largely comparable to that on cold carriers in the absence of EEF. As a result, their impact on PF *relative* enhancement is negligible. It is instead immediately detectable when comparing $\mu(T)$ in materials where EEF at interfaces is or is not in place. When GBs act as standard scattering centers, $\mu(T)$ is dominated by scattering at extended defects, with a weak dependence on T. Instead, when EEF is active, mobile (hot) carriers report a dependence of mobility fully comparable to those of single-crystals, since they do not sense intergrain potential barriers.[10]

As will be reported in Sec. V, most of the claims of EEF relate to multi-phase composites, whose micromorphology is set by preparation conditions, leading to a disordered location of interfaces. However, since barrier heights are set by the electronic structure of the phases and/or by the band folding at GBs, E_b is very weakly sensitive to disorder. Instead, composites display a statistical distribution of interbarrier spacings, whose effect on the transport properties must be accounted for. When spacing exceeds the carrier energy relaxation length λ_E, thermalization causes EEF-related PF enhancement to mostly fade away, with carriers recovering their standard mobility. When instead the spacing is smaller than λ_E, disorder was shown to just cancel out resonant tunneling, smoothing the dependence of the hot carrier mfp [and of $\tau(E)$ thereof] on their energy.[14] Strong validation of EEF is anyway more easily attained in nanostructured, top-down engineered thin films,[16] where optimal values of barrier spacing and heights can be controlled. The power factor of a Si-based nanodevice featuring multiple wells/barriers with $E_b = 160$ meV was experimentally measured to be 11 mW/mK^2, i.e., more than twice the PF achievable in bulk silicon at the same doping level. Furthermore, both the Seebeck coefficient and electrical conductivity were found to align well with EEF theoretical models. Since EEF theory is largely material-agnostic, the agreement between theory and experiment further corroborated the basic physics behind EEF.

C. Intrinsic energy filtering

The wording "intrinsic energy filtering" (IEF) was very recently introduced in two papers by Garmroudi *et al.*[13,17] and refers to the modulation of the relaxation time of carriers transitioning from overlapping flat and dispersive bands. Evidence of such an effect was showcased by the authors in NiAu alloys and in Ni_3Ge where localized, non-hybridizing states are present. Intrinsic energy filtering should not be confused with the effect of resonant state (RS) scattering. Resonant states are induced by dopants that create a sharp peak in the density of states around E_f, enhancing the Seebeck coefficient without significantly affecting electrical conductivity.[18] Although the outcomes of the two mechanisms are similar, namely, an increase in S without a corresponding drop in electrical conductivity, they deeply differ in their physical origin.

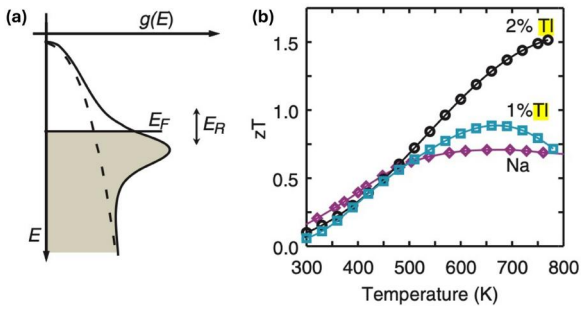

FIG. 1. (a) Comparison between the density of states of pure PbTe (dashed line) to that of Tl-doped PbTe (black line). (b) Figure of merit related to PbTe doped with 0, 1, and 2 at. % of Tl. Reprinted with permission from Heremans *et al.*, Science **321**, 554–557 (2008). Copyright 2008 AAAS.

In RS, the modulation of $g(E)$ takes place due to the presence of sharp peaks induced by localized states. Following the Mahan–Sofo theory,[19] Heremans *et al.* showed how a modification of the electronic structure of PbTe through the introduction of localized states associated with Tl dopants led to an increase in zT by a factor two[20] (Fig. 1). As IEF, also RS maximizes the transport distribution function $\Sigma(E) = q^2\nu^2(E)\tau(E)g(E)$ where $\nu(E)$ is the group velocity. In the case of RSs, however, the focus is on manipulating $g(E)$. When a dopant introduces a sharp resonance near the Fermi level, $g(E)$ increases drastically within a very narrow energy range. Thus, an increase in S follows, in accordance with Eq. (4). With IEF, instead, the approach aims to modulating $\tau(E)$ by engineering $\nu(E)$. The flatband provides a high $g(E)$ while the dispersive band provides high $\nu(E)$ (and mobility thereof). Filtering emerges because the scattering rate $\tau(E)^{-1}$ becomes extremely energy-dependent due to the transition probability between the two bands. When carriers approach E_f, the interband scattering suddenly turns on, cutting off the mobility of carriers. Thus, $\tau(E)$ shows up as a steep function of energy, making $\Sigma(E)$ strongly asymmetric. Since this does not require defects, the high metallic conductivity is preserved while IEF simultaneously boosts S—granting an enhanced power factor.

When interband scattering is mediated by phonons transferring their momentum to electrons, the temperature dependence of S is a landmark of IEF, reporting a sign reversal and a sudden increase above about $1/3$ of the material's Debye temperature, where $S(T)$ mirrors the temperature dependence of the phonon-assisted interband scattering rate. Note also that IEF does not involve any change of carrier density with temperature.

Concerning metallic alloys, an extended screening of the $g(E)$ of binary alloys pointed out how Ni alloys could meet the requirements for IEF to be observed.[17] Experimental analyses confirmed power factors with outstanding peak values of 34 mW/mK^2 at 560 K and of 29 mW/mK^2 at room temperature in metastable polycrystalline Ni_xAu_{1-x}, well mitigating the relatively large thermal conductivity ($\approx$50 W/mK) and thus yielding a zT of $\approx$0.3 at 560 K, an unprecedented figure of merit for a metallic system.

Also in Ni_3Ge, Garmroudi *et al.*[13] could confirm that metals exhibiting strong interband scattering and a large degree of band overlap can be employed as effective thermoelectric materials.[21] Also

05 May 2026 08:18:17

© Author(s) 2026

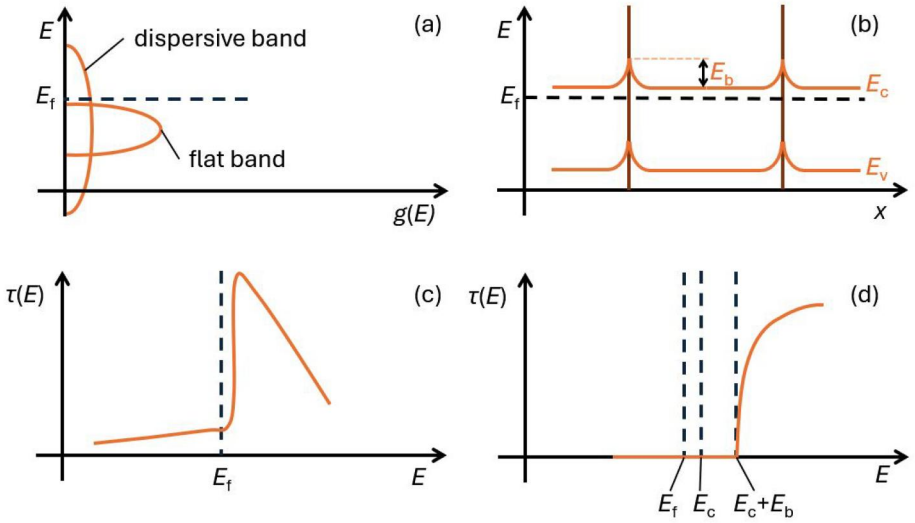

FIG. 2. Schematics of IEF and EEF. For IEF to be active, (a) flat and dispersive bands must overlap around the Fermi level. Instead, (b) EEF requires the presence of potential barriers blocking majority carriers with $E_c < E < E_c + E_b$. In both cases, carrier relaxation times $\tau(E)$ are modulated, sharply increasing for $E > E_f$ in IEF (c) and for $E > E_c + E_b$ in EEF (d).

in this case, filtering occurs within the flat (non-dispersive) band due to its overlap with dispersive bands. Since IEF is strongly dependent on the band structure, the authors developed a screening method based upon the density functional theory (DFT)-computed materials densities of states to identify systems that may exhibit IEF. Ni_3Ge was one of them. Polycrystalline Ni_3Ge samples were prepared using high-frequency induction melting and subsequently annealed at 973 K for several days. Samples showed a PF_{max} of 11 mW/mK^2 near room temperature along with a much lower thermal conductivity ($\approx$17 W/mK)—leading to a zT of about 0.2.

D. Comparing extrinsic and intrinsic energy filtering

As shown, although IEF and EEF rely on very different physics, both lead to an increase in carrier spectral relaxation time. Figure 2 pictorially summarizes the two mechanisms. As of their impact on thermoelectrics, IEF has recently been proved to disclose largely unexpected prospectives about the use of selected metallic alloys with a $L1_2$ structure (namely, a face-centered cubic structure with stoichiometry A_3B, where B atoms occupy the corner positions of the unit cell and A atoms occupy the face-centered positions)[17] to obtain high PFs. Extrinsic energy filtering is based instead on the introduction of a second phase (typically, a precipitate)—leading to the formation of a nanocomposite. As such, EEF may find implementation in largely different types of nonmetallic materials, ranging from small-gap semiconductors to large-gap oxides, and to polymers and organic materials as well. On the other hand, due to its weaker dependence upon the electronic structure of the host material, correct assignment of increased PF to EEF is often highly tentative. This is the main motivation for this review, suggesting criteria to take apart EEF from other phenomena that may enhance thermoelectrics and that might be confused with EEF.

III. UNDERSTANDING EXTRINSIC ENERGY FILTERING: FROM ROWE–MIN–WHITLOW–HIRANO MODEL TO MONTE CARLO SIMULATIONS

The first evidence of EEF in thermoelectrics dates back to 1990s, in two papers published by Rowe and Min[22] and by Whitlow and Hirano.[23] The concept of the two studies was different, yet converging. Rowe and Min studied the effect of multiple potential barriers on the thermoelectric properties of a homogeneous semiconductor through the relaxation-time approximation. Instead, Whitlow and Hirano proposed a theoretical analysis of the phenomenon in superlattices (SLs). In the former respect, despite the simplicity of the model, Rowe and Min confirmed that the presence of potential barriers could lead to an increase in the Seebeck coefficient. The impact of the reduced electrical conductivity, due to the decrease in carrier density, on the PF could be avoided by choosing a well-defined height of the barrier, such that the increase in the Seebeck coefficient overcompensated the reduction of σ, finally leading to a higher value of the PF

$$\frac{S_b^2\sigma_b}{S^2\sigma} = \frac{F_0(\xi - E_b)\left(\frac{2F_1(\xi-\epsilon_b)}{F_0(\xi-\epsilon_b)} + 2\epsilon_b - \xi\right)}{F_0(\xi)\left(\frac{2F_1(\xi)}{F_0(\xi)} - \epsilon\right)^2}, \tag{6}$$

where $F_j = (1/j!)\int_0^\infty z^j/(e^{z-x}+1)\mathrm{d}z$ are the Fermi integrals, $\epsilon = E/k_BT$ is the reduced energy, ξ is the reduced Fermi energy, and ϵ_b is the reduced barrier height. Note that the model assumes that charge carrier scattering is due to acoustic phonon scattering only.

Instead, Whitlow and Hirano advanced a model to estimate the effect of a superlattice structure on the density of states $g(E)$, evaluating both parallel and transverse conductivity, the latter sensing the presence of potential barriers. They moved from the standard model of heavily doped n-type SiGe. Assuming the complete localization of carriers with energy $E < E_b$, along with a 3D-like conduction for carriers with energy $E > E_b$, the model predicted a possible 100% increase in zT, compared to the bulk system.

Additional investigations by Nishio and Hirano[24] provided a formal theoretical analysis of EEF. In their paper, the authors provided an evaluation of the optimal barrier height and width. The former was determined to be $\Phi + qST$, where Φ is the chemical potential. Furthermore, Nishio and Hirano confirmed that the elimination of low-energy carriers is more significant in materials in which acoustic

05 May 2026 08:18:17

© Author(s) 2026

phonon scattering is dominant, as previously predicted by Rowe and Min.[22] Also the spacing d between barriers matter. On the one hand, it should be larger than the momentum relaxation length λ_p, enabling high-energy carriers to diffuse as they would in a system without barriers. On the other hand, d should be smaller than the energy relaxation length λ_E, avoiding relaxation (thermalization) of carriers.

Over the same years, experimental confirmations of these preliminary studies were provided. A high Seebeck coefficient of approximately 600 μV/K was obtained in polycrystalline $CoSb_3$ thin films,[25] in accordance with Rowe and Min[22] and Whitlow and Hirano[23] models. Furthermore, the importance of the microstructure was highlighted by Kishimoto *et al.*,[26] who studied the thermoelectric properties of PbTe films prepared by RF sputtering. They were able to find a relation between the effect of potential barriers and the GB structure. An increase in the Seebeck coefficient was observed in film with a columnar grain structure. Moreover, using the EEF model, they hypothesized a relation between localized states at GBs, resulting from defects, and the origin of the potential barriers. A barrier height of approximately 40 meV was measured, an optimal value which was confirmed in more recent publications.[10,27]

A remarkable contribution to the EEF theory came from Shakouri and Gossard,[28,29] highlighting the importance of the non-conservation of lateral momentum in a superlattice. They showed that, if lateral momentum is not conserved, a much larger number of *hot* carriers overcome the potential barriers (while filtering of cold carriers remains effective). Since the overall carrier density decreases, under these conditions, the Seebeck coefficient increases while the consequent decrease in electrical conductivity is partially compensated. Figures of merit up to 5 were predicted.[28]

Skepticism about EEF was brought instead by Heiliger and co-workers.[30] Their study focused on the effects of EEF at GBs in homogeneous semiconductors. Combining Seto's[15] and Green's[31] models, they predicted the transmission function of charge carriers through potential barriers at GBs. They concluded that, to enhance the power factor, a high chemical potential is required, and the barrier height should be within the same energy range. However, in a real system, to achieve these conditions a high carrier density is required, leading to a consequent screening by the Coulomb potential, making the barriers unable to filter low-energy charge carriers. This shows that the theoretical understanding of EEF mechanism had remained controversial. Nevertheless, once the potential enhancement of PF achievable through EEF was recognized, several more advanced theoretical models were developed for both polycrystalline and bulk materials.[32–34]

A sophisticated analyses of EEF were proposed by Neophytou *et al.* in two articles in the 2010s. In the first one, a theoretical study combining quantum mechanical DFT simulations with semi-classical transport analyses allowed the authors to evaluate tunneling and reflection effects caused by the presence of barriers. This led to optimize barrier characteristics for efficient EEF.[35] Specifically, it could be concluded that the width of the barrier should be large enough to suppress tunneling effects that would otherwise suppress S enhancement. Furthermore, the shape of the barrier was found to matter. Comparing smooth and square barriers, it was found that smooth barriers are more effective in enhancing thermoelectric properties. This theoretical prediction was used to perform an experimental study of thermoelectric properties of heavily boron-doped nanocrystalline silicon films.[36]

As mentioned, the growing number of theoretical models for EEF suggested practical guidelines for the effective design of new materials exploiting EEF. To face this challenge, Zianni and Narducci[37] developed a parametric model to estimate the effect of an energy barrier on the transport coefficient of a semiconductor as a function of the carrier concentration. First, they computed the transport coefficients using BTE within the relaxation time approximation. Then, approximating the transmission probability of charge carriers in the presence of potential barrier to a step function centered at E_b, only carriers with energy $E > E_b$ can participate in the transport mechanism. The authors were able to derive approximate expressions for the ratios of the electrical conductivity and Seebeck coefficients in the presence of potential barriers compared to the conductivity and Seebeck coefficient of the bulk semiconductor. They found that such ratios depend only on the reduced barrier height ϵ_b, the reduced Fermi energy ϵ_f and the exponent describing the dominating carrier scattering mechanism, enabling a simple correlation between the system characteristics and the observed EEF-related enhancement by using analytical expressions.

By the end of 2010s, it became clear that improving PF through EEF required:

1. A barrier width large enough to suppress tunneling effects.
2. An interbarrier spacing smaller than the carrier mfp in the pertinent material, therefore preventing thermalization of carriers between barriers.
3. A barrier height typically between $k_B T$ and $2k_B T$. This makes the fraction of filtered carriers ranging from about 60% to 75% in a strongly degenerate semiconductor, and from about 65% to 85% in a non-degenerate one—i.e., high enough to filter out a substantial fraction of carriers, yet not indiscriminately scattering all carriers.
4. A high carrier density ($\sim 10^{19} - 10^{20}$ cm^{-3}), to keep the density of mobile carriers large enough not to dampen the electrical conductivity too much.

Failure to fully meet such criteria are responsible for inefficient when not fully ineffective extrinsic energy filtering, often leading to a reduction of PF due to energy-independent carrier scattering at inner interfaces.

An additional benefit may come to implement EEF along with a modulation doping approach. This last point was elucidated by Neophytou *et al.*,[38] who highlighted the importance of carrier mobility in the presence of high dopant densities. The authors proposed a mechanism where carriers flow from heavily doped regions into undoped regions with barriers. These dopant-free regions allow for a higher mfp for high energy carriers, leading to an increase in $\mu(E)$, thus further mitigating the reduction in electrical conductivity.

The importance of carrier mobility was further elucidated in a paper published in 2024 by Priyadarshi *et al.*[39] Their aim was to overcome the approximations of previous models by employing advanced Monte Carlo simulations coupled with the Poisson equation. Specifically, the authors accounted for phonon scattering as well as ionized impurity scattering, confirming that, with precise system design, EEF could enhance the Seebeck coefficient without compromising the electrical conductivity.

05 May 2026 08:18:17

© Author(s) 2026

IV. EXTRINSIC ENERGY FILTERING DISTINCTIVE FEATURES: A GUIDE TO EXPERIMENTALISTS

In Sec. III, we reported the most relevant achievements in the study of the EEF physics. The aim of this section is to provide a practical guide to experimentalists, to facilitate both the design of new materials and the identification of EEF among the various phenomena that enhance thermoelectric properties. The main challenge lies in identifying the key ingredients required for EEF, since *anomalously higher PF values are not always indicative of EEF activation*.

Activation of EEF requires a fine control and optimization of several parameters to make this phenomenon beneficial to the material.[35–37,40,41] In turn, this can be used to validate the occurrence of EEF. There are two main approaches that can be followed to this aim.

The most intuitive path involves microscopic-level characterization. In particular, imaging by scanning electron microscopy (SEM) or transmission electron microscopy (TEM) combined with electron energy loss spectroscopy (EELS) can confirm the presence and estimate the height of potential barriers at interfaces or grain boundaries. Such evidence, coupled with improved thermoelectric properties, is a strong indicator of EEF. Figure 3 shows an example of TEM and dark-field scanning electron transmission microscopy (DF-STEM) confirming the presence of a second phase at GBs due to dopant precipitation.[42] Angle-resolved photoemission spectroscopy (ARPES) can be also used to reveal localized states or band bending that may confirm or rule out EEF, as it allows for a detailed mapping of the electronic structure. Although not widely employed in the study of EEF, ARPES provides fundamental information for identifying the presence of the filtering effect.[43]

Despite their strong potential for identifying EEF effect, electron microscopy and ARPES require long preparation and are time consuming. Alternative methods can be used to identify EEF in a given system, however. They include the analysis of μ as a function of temperature and of Pisarenko's plot. To understand how to make use of such techniques, let us consider Mott's equation, which describes the effect of increase in $g(E)$ on the Seebeck coefficient[20]

$$S = \frac{\pi^2 k_B}{3q} k_B T \left\{ \frac{1}{n}\frac{dn(E)}{dE} + \frac{1}{\mu}\frac{d\mu(E)}{dE} \right\}_{E=E_f}. \quad (7)$$

It shows that there are two main contributions to S: the energy dependence of the carrier density $n(E)$ and of the mobility $\mu(E)$. Extrinsic energy filtering typically introduces a cutoff energy, below which charge carriers are reflected or scattered. Thus, by measuring μ as a function of T by Hall effect measurements, one extracts $\mu(E)$ and estimate the barrier height. Furthermore, the dependence of S on $n(E)$ can be expressed in terms of the effective mass as

$$S = \frac{8\pi^2 k_B^2 T}{3qh^2} m^* \left(\frac{\pi}{3n}\right)^{2/3}. \quad (8)$$

Since S decreases when the carrier density increases, a Seebeck coefficient that deviates from this trend provides a strong evidence of EEF.

Figure 4 shows a Pisarenko's plot, displaying S as a function of the carrier density. As mentioned, S decreases with increasing carrier density (solid line). If experimental data deviate from this behavior (black dots), this implies an additional scattering mechanism that enhances the Seebeck coefficient, such as EEF. This indicator, when combined with improved transport properties or TEM images, can be used to confidently confirm the occurrence of EEF.

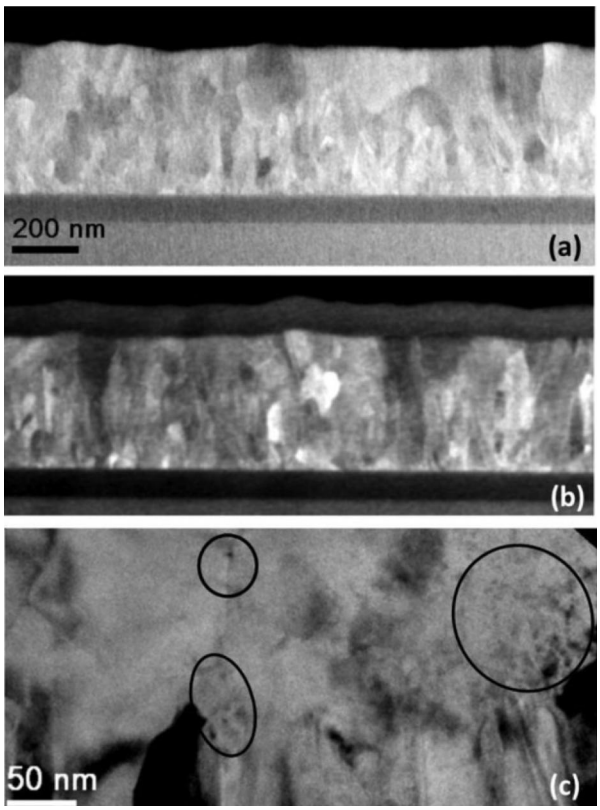

FIG. 3. DF-STEM of a nanocrystalline thin silicon film (a) as deposit and (b) after annealing at 1000 °C. Black circle in TEM image (c) highlights diffraction contrast due to the presence of a second phase at grain boundaries acting as potential barriers. Reprinted with permission from Narducci *et al.*, Physica Status Solidi A **211**, 1255–1258 (2014). Copyright 2014 Wiley.

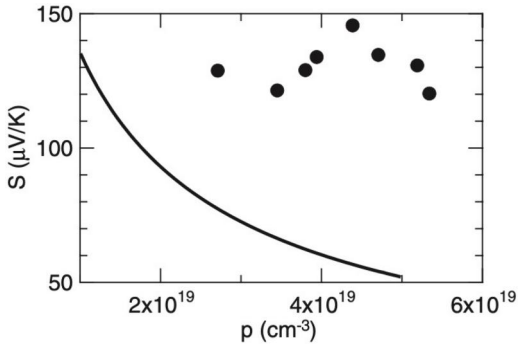

FIG. 4. Schematic representation of the standard behavior of S as a function carrier concentration (black line). Experimental S values that deviate from this model (black dots) may indicate the presence of additional scattering mechanism. Reprinted with permission from Heremans *et al.*, Science **321**, 554–557 (2008). Copyright 2008 AAAS.

05 May 2026 08:18:17

© Author(s) 2026

Equation (7) is also useful to explain another important way to identify EEF: the dependence of σ and S on temperature. In general, filtering effects are temperature-sensitive, meaning that the effect can be more or less pronounced as a function of T. A barrier with height E_b can be obviously crossed only by carriers with $E > E_b$. By increasing the temperature, the fraction of carriers overcoming the barrier increases, leading to an increase in σ. Concerning the Seebeck coefficient, an increase in carrier density n should lead to a decrease in $|S|$. However, such an increase is small, if the barrier is $\approx 2k_B T$ in the temperature range where the material is to be used. Therefore, the increase in $n(T)$ is overcompensated by the linear dependence of the Seebeck coefficient on T [cf. Eq. (8)]. Thus, *over the temperature range the material is supposed to operate*, both σ and $|S|$ increase with the temperature. Thus, from a practical point of view, by measuring $\sigma(T)$ and $S(T)$, a *simultaneous* increase in both σ and S generally indicates the occurrence of EEF.

In summary, the main tools/criteria to identify EEF are:

1. Scanning or transmission electron microscopy (SEM, TEM, or DF-STEM) possibly coupled with EELS, to obtain visual evidence about the presence of potential barriers (second phase precipitates) and an estimate of the value of its height.
2. Angle-resolved photoemission spectroscopy (ARPES), to obtain a detailed map of the materials electronic structure, allowing for the identification of band bending.
3. Variable-temperature Hall effect measurements, to evaluate $\mu(E)$ and $n(E)$, enabling the estimate of barrier height.
4. Comparison of experimental data (S and n) with the Pisarenko's plot, to detect deviations from the standard linear trend—revealing a scattering mechanism that enhances the Seebeck coefficient.
5. Electrical conductivity and Seebeck coefficient measurements as a function of temperature, to verify whether an increase of temperature leads to a simultaneous increase of both σ and S—due to the higher hot carrier density overcoming the barriers and to the filtering of low-energy carriers.

We stress once again that the verification of a single criterion should not be considered sufficient to assess EEF.

V. EXTRINSIC ENERGY FILTERING IN THERMOELECTRIC MATERIALS

In this section, we will give the reader an overview of recent developments about the implementation of EEF in crystalline system, including elemental semiconductors, chalcogenides, and oxides.

A. Extrinsic energy filtering in chalcogenides

As well known, several of the best thermoelectric materials are tellurium-based. Among them, PbTe and Bi_2Te_3 are the most studied.

One of the first paper addressing EEF in tellurides dates to 2012, when energy filtering due to anisotropic interfaces and grain boundaries in bulk $Bi_2Te_{3-x}Se_x$ nanoplatelet composites submitted to spark-plasma sintering (SPS).[44,45]

In more recent years, Zhong *et al.*[46] reported EEF as leading to a maximum value of zT around 2.5 for p-type PbTe. However, despite the significant improvements, the n-type counterpart still exhibited a much lower zT. Figure 5 summarizes the improvement of both peak

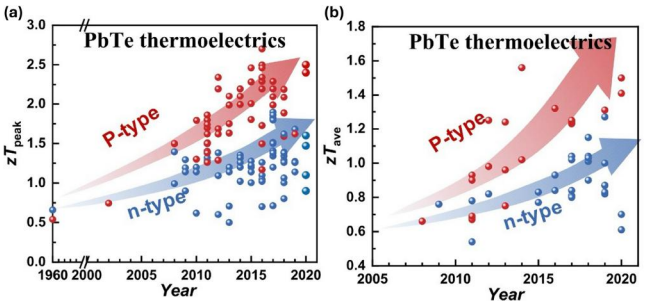

FIG. 5. (a) Peak figure of merit (zT_{peak}) and (b) average figure of merit (zT_{ave}) for both p-type and n-type PbTe thermoelectric. Reprinted with permission from Zhong *et al.*, ACS Appl. Mater. Interfaces **12**, 49323–49334 (2020). Copyright 2020 American Chemical Society.

zT_{peak} and average zT_{ave}. Comparable considerations hold true for other tellurides.

This is due to the different electronic structure of valence and conduction bands, computed by DFT, which leads to lower PF value of n-type legs compared to p-type legs. Energy filtering has been considered as possible solution to enhance the PF of n-type telluride-based materials, but also to further enhance the performance of p-type legs.

Kawajiri and co-workers[47] reported a successful activation of EEF in n-type $Bi_2Te_{3-x}Sb_x$ by adding gold through ultrasonication or ball-milling followed by spark-plasma sintering—leading to a zT 75% higher than the gold-free material. The electronic structure of the system lets understand how gold promotes EEF. A potential barrier of 0.07 eV is formed at the metal–semiconductor junction according to Schottky's model. That barrier generates an electron accumulation region filtering out low-energy carriers. TEM images of $Bi_2Te_{3-x}Sb_x$ confirmed the presence of both Au and of a third phase ($AuTe_2$), which may also help promote EEF.

Zhang *et al.*[48] achieved a zT value of 1.83 at 773 K by incorporating InSb into n-type PbTe through high-energy ball milling, resulting in a multiphase nanostructured material. Moreover, the multiple interface formed between InSb and matrix gave place to hierarchical potential barriers capable of filtering out low-energy carriers at different temperatures. Specifically, authors detected a barrier with $E_b \sim 50$ meV at the Sb/PbTe interface, effective at 300 K, a higher barrier ($E_b \sim 250 - 300$ meV) at Pb/Sb and InSb/PbTe interfaces, operating around 450–600 K, and a barrier with $E_b \sim 480$ meV at the In/PbTe interface, suitable for filtering around 750 K. Note how different barrier heights are needed to enable EEF over different temperature ranges.

Liu *et al.*[49] achieved a zT peak value of 1.5 at 773 K by introducing Ag_2Te into n-type $Pb_{0.975}Cr_{0.025}Te$. Two key ingredients contribute to the high zT value. On one hand, the dynamic doping of silver, namely, the concurrent effect of the heterovalent doping by Ag and of the temperature-dependent solubility of Ag_2Te, causes the carrier density and the formation of Ag_2Te precipitates (and interfaces, thereof) to be temperature-modulated. On the other hand, precipitates enables the optimization of phonon scattering by Ag_2Te second phases. The capability of Ag embedded in nanodots or heterostructures was known to filter out minority carriers,[50] uncompensating

05 May 2026 08:18:17

© Author(s) 2026

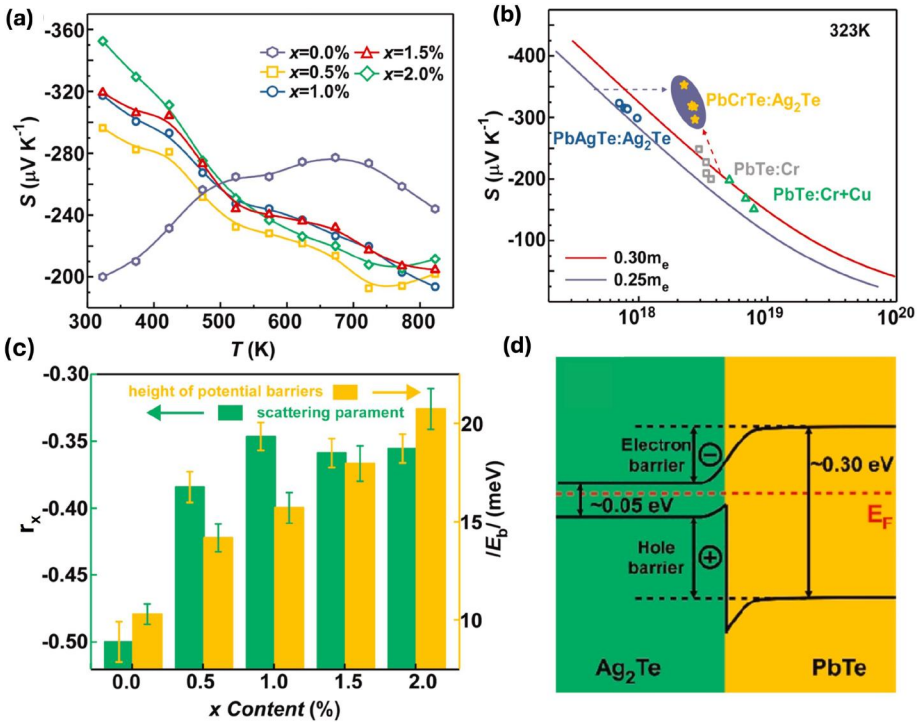

FIG. 6. (a) Temperature dependent Seebeck coefficient of $(1-x)Pb_{0.975}Cr_{0.025}Te$-$xAg_2Te$ ($x = 0$, 0.5%, 1.0%, 1.5%, 2.0%); (b) Pisarenko's plot of different PbTe composite materials. Note how Seebeck coefficient values of PbCrTe:Ag_2Te are higher compared to theoretical predictions; (c) barrier height E_b and scattering parameter r_x as a function of Ag_2Te content; (d) schematic band diagram explaining the origin of the potential barriers at the Ag_2Te/PbTe interface. Reprinted with permission from Liu *et al.*, Nano Energy **91**, 106706 (2022). Copyright 2022 Elsevier.

majority carriers by EEF. Several $(1-x)Pb_{0.975}Cr_{0.025}Te - xAg_2Te$ compounds were prepared via vacuum melting followed by hot pressing to confirm the role of Ag in the alloys.

Figure 6 shows that a significant increase in the Seebeck coefficient near room temperature could be observed for samples containing Ag_2Te, compared to those without dopant [Fig. 6(a)]. This enhancement could be attributed either to EEF but also to changes in the band structure. To investigate possible modifications in the band structures, the Single Kane Band (SKB) model was used [Fig. 6(b)]. Both PbAgTe:Ag_2Te and PbTe:Cr well fit Pisarenko's line assuming respectively effective masses of $0.25m_e$ and $0.30m_e$. This trend indicates that the band structure is not significantly altered by the presence of Ag. Therefore, Ag must form nanoprecipitates acting as scattering sources at the matrix-precipitate interface, giving rise to EEF. As a further confirmation, the scattering parameter (r_x) was analyzed as a function of Ag_2Te content, showing that higher Ag_2Te concentrations correspond to higher r_x values [Fig. 6(c)]. Moreover, the potential barrier height at the interfaces was estimated as

$$\sigma \propto T^{1/2} \exp\left(-\frac{E_b}{k_B T}\right). \tag{9}$$

It was found that the barrier height increases with the Ag_2Te content, showing how higher dopant contents lead to higher barrier heights, consistent with previous evidence related to interface sites [Fig. 6(c)]. Finally, Fig. 6(d) reports the band alignment between Ag_2Te and PbTe. A potential barrier is formed for both holes and electrons at the interface, due to the mismatch between conduction and valence band in the two phases. This leads to the scattering of low-energy carriers and, consequently, to an increase in the Seebeck coefficient, further confirming the occurrence of EEF.

Based on the same concepts, another remarkable work was published by Cho *et al.*[51] in 2020. Once again, the authors aimed to improve the thermoelectric properties of Bi–Te systems using the EEF approach. In detail, they investigated thermoelectric properties of $(CuI)_{0.003}Bi_2Te_{2.7}Se_{0.3}$–Mo composites, with different amounts of molybdenum. The idea of activating EEF effects is promoted by the difference between the work functions of Mo (4.36–4.95 eV) and of Bi–Te alloys (5.1–5.4 eV), which facilitates the formation of potential barriers filtering out low-energy carriers. The composites were prepared by mechanical ball-milling of $(CuI)Bi_2TeSe$ ingots with Mo nanopowders followed by hot-press sintering. One of the most important difference with respect to previous works concerns the thermal conductivity, which is usually reduced by the presence of a second phase. Instead, as shown in Fig. 7(a), κ_{lat} values of Mo-dispersed samples are similar when not higher than those of the pristine material. This unexpected feature found an explanation considering that additional phonon scattering by a second phase depends on the particle size. In this study, Mo particles have sizes of several μm. Thus, they do not significantly affect phonon mfp. Nevertheless, the increase in the PF lets the zT value of Mo-dispersed composites be strongly enhanced compared to the pristine material around room temperature, up to 1.02 at 373 K [Fig. 7(b)].

The EEF approach has also been investigated to further enhance p-type leg zT. In 2018s, Pakdel *et al.*,[52] carried out an experimental study aiming at the improvement of the thermoelectric performances of p-type $(1-x)Bi_{0.5}Sb_{1.5}Te_3 - xSb_2O_3$, also considering its stability over a period of 24 months. The composites were synthesized starting from stoichiometric amounts of Bi, Sb, and Te powders, melted

05 May 2026 08:18:17

© Author(s) 2026

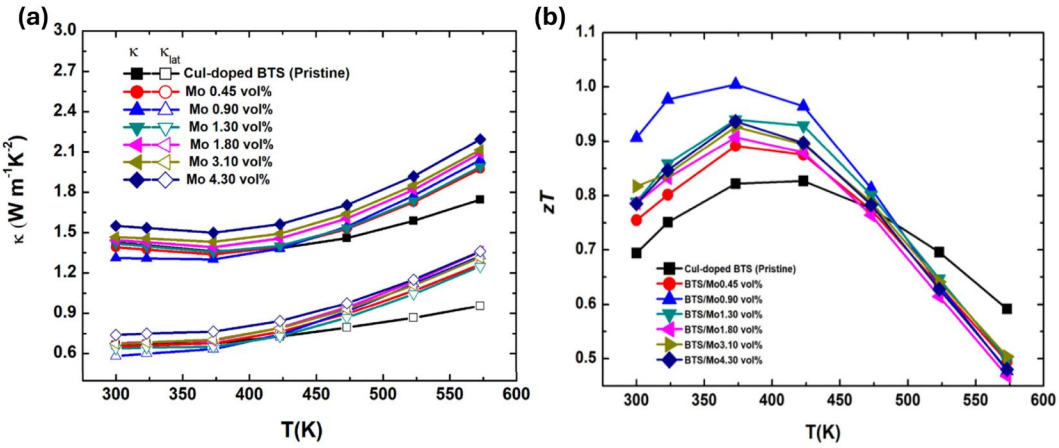

FIG. 7. (a) Lattice (empty markers) and total (filled markers) thermal conductivity and (b) temperature dependent zT values of $(1-x)(CuI)_{0.003}Bi_2Te_{2.7}Se_{0.3}$-$x$Mo ($x = 0$, 0.45, 0.9, 1.3, 1.8, 3.1, and 4.3 vol. %). Reprinted with permission from Cho *et al.*, ACS Appl. Mater. Interfaces **12**, 38076–38084 (2020). Copyright 2020 American Chemical Society.

together and then ball milled. The Sb_2O_3 nanoparticles were then mixed with Bi–Sb–Te powders and spark plasma sintered. With the introduction of Sb_2O_3 nanoparticles, the authors observed a decrease in the electrical conductivity. Although an increase in μ was observed, it was not sufficient to compensate the reduction of the carrier density. However, the decrease in σ was more than compensated by a significant enhancement of the Seebeck coefficient due to low-energy hole filtering. As a result, a zT peak value of 1.51 at 300 K was achieved in the composite with 4 wt. % of Sb_2O_3. Regarding zT stability in time, the performance of the composites declined by only about 6.6% over a period of 24 months, confirming the excellent stability of the synthesized composites.

Among all chalcogenides, Te-based compounds show the best thermoelectric performance. Nevertheless, in recent years, other chalcogenides have attracted the attention of the scientific community. Selenium-based materials are particularly promising due to their low κ value.[53] Also in this case, the possibility of implementing EEF has been explored.[54,55] Lu *et al.*[54] studied the influence of Cu doping on the thermoelectric properties of Ag_2Se composite films, also evaluating their possible integration into flexible devices. TEM analysis confirmed the presence of Ag and AgCuSe precipitates at the grain boundaries of the matrix. As a result, low-energy carriers were filtered out, achieving a PF value of $\approx$2.2 mW/mK^2 at 300 K. Nanostructured SnSe has also been investigated for high-temperature applications.[55] A remarkable zT value of 2.0 at 873 K was achieved in composites embedding Se quantum dots (QDs) into a $Sn_{0.99}Pb_{0.01}Se$ matrix that were obtained by magnetic field-assisted hydrothermal synthesis. The advantage of this technique lies in the formation of a homogeneous distribution of Se quantum dots and PbSe nanoprecipitates. The Se QDs are found to enhance the density of states around E_f (as confirmed by ultraviolet photoelectron spectroscopy) and, moreover, they introduce multiple potential barriers in the matrix, leading to an efficient filtering of low-energy carriers.

Still on Te-based materials, Ma *et al.*[56] introduced BiCuSeO@SnO_2 core shell nanoparticles into a SnTe matrix by high-temperature solid state reaction. As shell components and due to its large bandgap (3.59 eV), SnO_2 forms potential barriers between the matrix and the BiCuSeO core, inducing the EEF effect. TEM images confirmed the presence of the shell and, consequently, the existence of potentials barriers. Moreover, Hall analysis were crucial to identify EEF. Carrier concentration gradually decreases by increasing the BiCuSeO content, while mobility increased up to 350% compared to the undoped sample. Consistently, the Seebeck coefficient of doped samples gradually increased with temperature. Furthermore, Pisarenko's plot showed that experimental values of S for the doped samples lie above the Pisarenko's line. As reported in Sec. IV, all evidence are strong indicators of the occurrence of EEF. Since in this case also the thermal conductivity decreased down to a minimum value of 1.04 W/mK in $Sn_{1.03}Te$–5% BiCuSeO, a notable zT value of 1.21 could be achieved at 835 K, a value 190% higher than that of pristine SnTe.

Extrinsic energy filtering was also reported enhancing efficiency in materials exploiting the thermoelectromagnetic effect. Magnetic impurities were reported to increase Seebeck coefficient even where no EEF is active.[57,58] Furthermore, Yan *et al.* showed how the thermoelectromagnetic coupling effect can be induced also by the introduction of magnetic nanoparticles into bulk thermoelectric materials.[59] Filtering cooperates with the thermoelectromagnetic effect when ferromagnetic Co particles are inserted into $Bi_{0.5}Sb_{1.5}Te_3$–polyvinylidene fluoride films. Remarkably, while σ increases, the Seebeck coefficient remains almost unchanged, indicating that the introduction of Co particles impact the scattering mechanism, partly due to the carrier energy filtering effect at the heterointerface.

Sulfides are also promising materials in the medium-temperature range (373 K $< T <$ 800 K), with the additional advantage of being based on geo-abundant elements (differently from tellurides) and of being nontoxic (differently from selenides). In recent years, research has focused on a specific class of sulfur-based materials, namely, Cu_xS ($1 \leq x \leq 2$) and its derivatives. These materials show Cu vacancies acting as acceptors, being then p-type semiconductors with a bandgap energy between 1.2 and 1.5 eV. Some of the most studied sulfur-based thermoelectric materials are SnS,[60] tetrahedrites,[61] Cu_2S,[62] and PbS.[63] Due to their structure, these materials are versatile and can be doped and engineered into hierarchical

05 May 2026 08:18:17

© Author(s) 2026

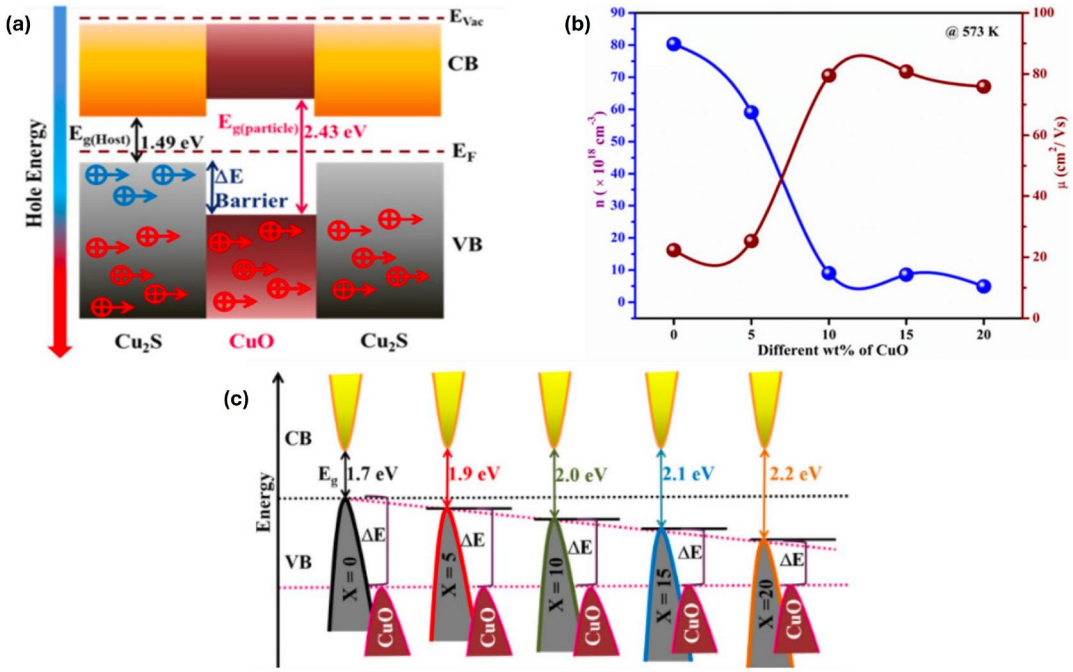

FIG. 8. (a) Band alignment at the Cu_2S/CuO interface, due to the wideband gap of CuO, low-energy charge carriers are filtered out at the interface. (b) Hall mobility and carrier concentration as a function of CuO wt. % and (c) effect of the amount of CuO on the band structure. Reprinted with permission from Mani *et al.*, J. Inorg. Organomet. Polym. Mater. **34**, 1548–1563 (2024). Copyright 2024 Springer.

structures. Although analyses are currently incomplete, several studies carried out on sulfides suggest the potential application of EEF in these systems.

In a recent study, Mani *et al.* prepared Cu_2S composites embedded with CuO nanoparticles, an oxide with a wide bandgap (∼2.5 eV). Cu_2S and CuO nanoparticles were synthesized respectively via solvothermal and hydrothermal processes and subsequently mixed to form nanocomposites with different wt. % of CuO.[64] Due to the combined effects of EEF and phonon scattering at the Cu_2S–CuO interfaces, a Seebeck coefficient 71.45% higher than the pristine material could be achieved, along with a 61.6% reduction in thermal conductivity. Figure 8(a) shows a schematic representation of the band alignment after the incorporation of CuO nanoparticles. At the Cu_2S–CuO interfaces, potential barriers filtering out low-energy holes are formed. This mechanism leads to the aforementioned *S* enhancement, accompanied by a carrier density reduction and an increase in mobility [Fig. 8(b)]. Despite the mobility enhancement, however, the electrical conductivity of the composites decreased. This can be easily understood in view of the band structure of the composites at different wt. % of CuO [Fig. 8(c)]: the higher the CuO content in the composites, the larger the bandgap, increasing from 1.7 eV for 0 wt. % to 2.2 eV for 20 wt. %. This notwithstanding, the coupled effect of EEF and phonon scattering returned a zT value of 0.44 for the Cu_2S–CuO 15 wt. % composite, namely, a value 214.3% higher than the pristine material.

Chen *et al.* were able to obtain multiscale architectures of $Cu_{2-x}S$ through the mechanical mixing of nano- and microparticles (of the same material) followed by SPS processing.[65] They highlighted the fundamental role of grain boundaries. The introduction of nanoparticles led to the formation of new interfaces between the micro- and nano-phases that could be used as a key feature to elicit EEF.

Nanopores may operate to activate EEF too. Luo *et al.* studied by DFT the effect of $CdCl_2$ and $ZnCl_2$ doping on the band structure of $CuGaTe_2$.[66] They found that the increased carrier density did not negatively impact the Seebeck coefficient because of nanoholes formed by the release of Cl_2 upon heat treatments, blocking low-energy carriers. A doubled PF was reported that, along with the beneficial phonon scattering by nanoholes, led to a zT of 1.4 at 800 K in $(CuGaTe_2)_{0.985}(ZnCl_2)_{0.015}$. This quite aligns with the observation of a comparable beneficial effect of nanovoids (with a diameter of ≈3 nm) in polycrystalline Si thin films.[67]

B. Extrinsic energy filtering in oxides

Among the motivations leading researchers to study new thermoelectric material is to develop materials that are abundant, low-cost and nontoxic. Oxides meet all these requirements, and are also suitable for high-temperature applications in air, differently from other materials not withstanding oxidizing conditions. Once again, the main drawback of using oxides as thermoelectric materials lies in their transport properties, which are typically characterized by low electrical conductivity and high thermal conductivity.[68] Some of the most studied oxides for thermoelectricity include NiO,[69] ZnO,[70] Cu_xO,[71] In_2O_3,[72] and $NaCo_2O_4$.[73]

Regarding the EEF effect, Gayner *et al.*[74] studied the possibility of improving the thermoelectric properties of ZnO by co-doping with Al and Ti. Authors studied the effect of doping by preparing

05 May 2026 08:18:17

© Author(s) 2026

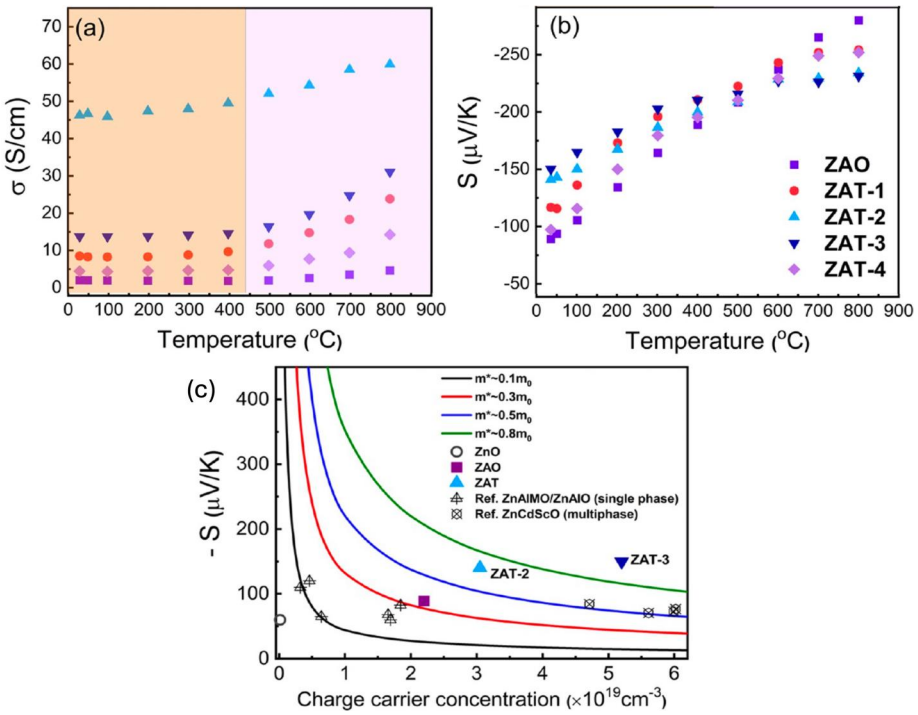

FIG. 9. Temperature dependence (a) electrical conductivity and (b) Seebeck coefficient for $ZnAl_{0.02}O$ with 1, 2, 3 and 4 wt. % of TiO_2. (c) Pisarenko's plot of co-doped samples, compared with other single phase and multiphase materials. Reprinted with permission from Gayner *et al.*, ACS Appl. Mater. Interfaces **14**, 4035–4050 (2022). Copyright 2022 American Chemical Society.

$Zn_{0.98}Al_{0.02}O$, $Zn_{0.98}Ti_{0.02}O$, and $Zn_{0.98}Al_{0.02}O$ with 1, 2, 3, and 4 wt. % of TiO_2. Figure 9 shows $\sigma(T)$ and $S(T)$ for the different samples, all of which exhibiting semiconducting behavior across the entire temperature range. Interestingly, the Ti-doped samples shows a Seebeck coefficient up to 1.5× higher than the undoped sample, suggesting that three-phase materials has better thermoelectric properties than the two-phase one. Figure 9(c) shows an increment in the electron effective masses in Al- and Ti-doped samples (green and blue lines) compared to the reference single phase (ZnAlO) and multiphase (ZnCdScO) which may be the reason for the higher S values. Furthermore, the deviation from Pisarenko's plots [Fig. 9(c)] shows how the enhanced Seebeck coefficient observed in specimens with 2 and 3 wt. % TiO_2 arises from the energy filtering effect.

C. Extrinsic energy filtering in group IV semiconductors

Research on thermoelectric materials focused on low-cost and highly geo-available materials has naturally met silicon and its alloys. Despite its poor thermoelectric properties as single crystal, silicon can be a competitive solution for low-temperature heat harvesting applications.[75] The main drawback of silicon as the thermoelectric material lies in its very high thermal conductivity (∼152 W/mK at room temperature) that reduces its zT down to 0.01, a value too low to compete with other materials.

Early evidence of an anomalous simultaneous increase in σ and S in Si upon annealing were reported by Vining in the late 1980s[76,77] and further confirmed by Loughin *et al.*[78] in boron-doped SiGe alloys. In both cases, boron precipitation at grain boundaries was considered as the cause of the anomaly, although no physical explanation was advanced. More than 15 years later, Dresselhaus and co-workers reported a small but detectable increase in the power factor in boron-doped SiGe pellets, once again ascribing it to SiB_x precipitates at grain boundaries.[79,80] A more systematic investigation of EEF effects in silicon thin films was carried out by Narducci and co-workers.[27] Moving from the experimental evidence of a concurrent increase in the Seebeck coefficient and of the electrical conductivity upon sequential annealing of heavily boron-doped silicon,[81] the authors advanced the hypothesis that such power factor enhancement could be related to EEF.[14] To corroborate such conjecture, nanocrystalline silicon thin films were deposited via chemical vapor deposition (CVD).[42] The doping processes were carried out by ion implantation to obtain boron hyper-doped, degenerate silicon, with nominal boron concentrations of about 4×10^{20} cm^{-3}, close to boron solubility threshold at 1000 °C. After damage recovering, samples were submitted to a high-temperature annealing process up to 1000 °C in argon to allow boron diffusion and precipitation at GBs. Samples with boron content below 4×10^{20} cm^{-3} did not show boron precipitation and consequently exhibited no increase in the mobility or in the PF. On the other hand, Hall effect measurements and TEM analyses confirmed that annealing processes at temperature $\geq$800 °C resulted in the precipitation of a second phase (SiB_x) in samples with boron content $\geq 4 \times 10^{20}$ cm^{-3}. This led to an increase in S and μ, compensating the reduction of carrier density on σ, in agreement with theoretical models.[82] Power factor values of ∼15 W/mK^2 were reported. In a more recent publication, the same collaboration studied the role played by hydrogen in partially deactivating EEF.[10] Infrared reflectance spectroscopy confirmed the presence of hydrogen (as a by-product of silane decomposition).

Figure 10 shows the spectra of non-implanted samples, as well as implanted samples before and after annealing. Authors were able to conclude that only when hydrogen is successfully removed from the

05 May 2026 08:18:17

© Author(s) 2026

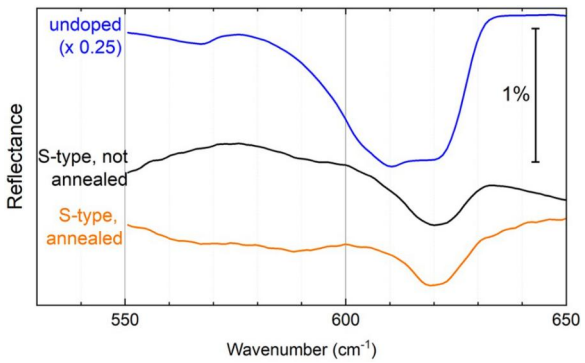

FIG. 10. FT-IR reflectance spectra of undoped and boron doped thin films before and after the annealing. The strong signal at 620 cm^{-1} is related to the Si–H wagging vibrational mode. Upon implantation the intensity of the Si–H peak decrease due to the higher affinity of H for B forming BH_x complexes. The annealing cause the outdiffusion of H from both BH_x and Si–H bond. Reprinted with permission from Narducci *et al.*, Appl. Phys. Lett. **119**, 263903 (2021). Copyright 2021 American Institute of Physics.

samples (through thermal treatments or room temperature aging), the annealing process leads to the full precipitation of SiB_x second phase at grain boundaries, enabling enhanced low-energy hole filtering. Combining the exceptionally high PF of ∼33 mW/mK^2 achievable upon hydrogen removal with a computationally estimated thermal conductivity of 10 W/mK, a zT of 0.99 was estimated at room temperature, making Si a competitive option compared to other high-performance thermoelectric material, also considering its abundance, low cost, and nontoxicity.

Filtering in Si may be also induced by extended defects. Bennett and co-workers showcased a simultaneous increase in σ and S in single-crystalline Si films that was ion-implanted with ^{28}Si ions at a beam energy of 2 MeV, inducing a large density of dislocations.[83] Although no final conclusion was drawn, activation of EEF was put forward as a possible cause for the enhanced PF, increased by ≈70%.

D. Extrinsic energy filtering in composites

Hybrid organic–inorganic materials have attracted the interest of the thermoelectric community due to the low thermal conductivity and relatively high Seebeck coefficient of the organic component, coupled with the high electrical conductivity of the inorganic component.[84,85] Energy filtering has been extensively studied in hybrid organic–inorganic materials with the purpose of improving such trade-off between Seebeck coefficient and electrical conductivity.[86] Still, the real EEF capabilities of boosting thermoelectric properties remains under scrutiny.

Liang *et al.*[87] critically examined the role of energy filtering in poly(3-hexylthiophene)-Te nanowires (P3HT-TeNWs) composites by systematically tuning the barrier height from 0.08 to 0.88 eV. Although high power factors were achieved with both low and high barrier energies, authors were able to explain the measured Seebeck coefficient values without invoking EEF, suggesting that EEF may not be the dominant mechanism behind the observed enhancement. This

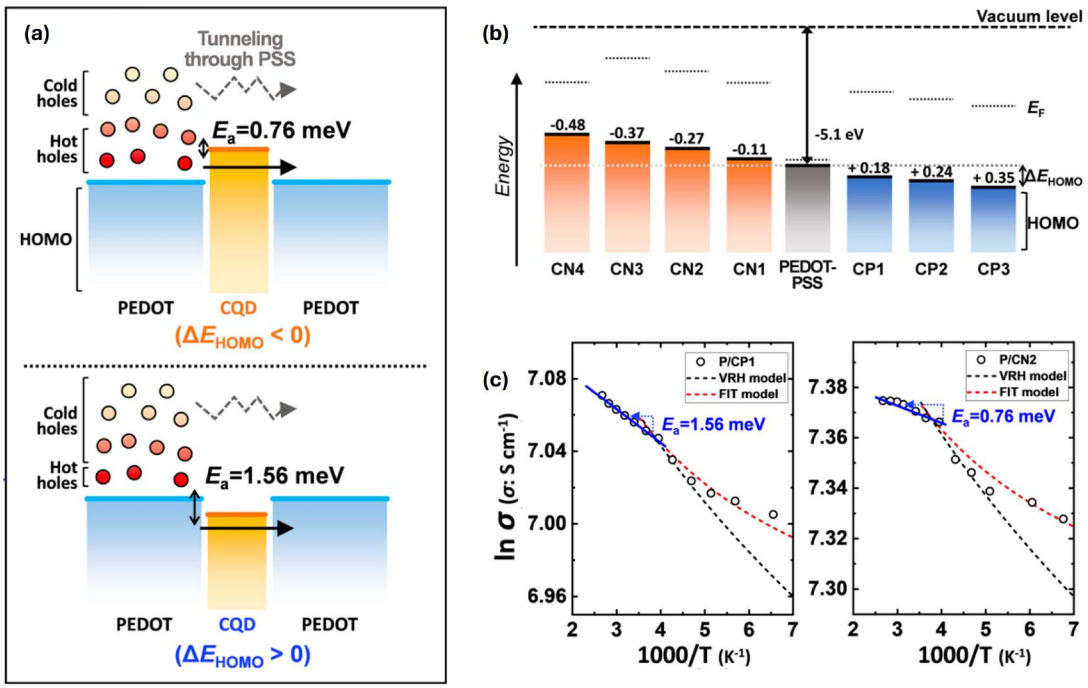

FIG. 11. (a) Schemes of the filtering process due to the presence of CQDs: charge carriers, depending on their energy, can move from PEDOT to PSS or CDQs. (b) ΔE_{HOMO} of composite material and (c) the variable-range hopping (VHR) model failed to describe the σ data the hybrid materials, indicating that took place a different conduction mechanism. Reprinted with permission from Kim *et al.*, Chem. Mater. **33**, 4853–4862 (2021). Copyright 2021 American Chemical Society.

05 May 2026 08:18:17

© Author(s) 2026

observation is further supported by the fact that the maximum power factor was achieved at a barrier height of 0.88 eV, a too high E_b to attain an efficient filtering of low-energy carriers.

Instead, Kim *et al.*[88] studied the effects of incorporating semiconducting carbon quantum dots (CQDs) into poly(3,4ethylenedioxythiophene):polystyrene sulfonate (PEDOT:PSS) nanocomposites. By precisely engineering the surface states, the authors were able to prepare CQDs with different highest occupied molecular orbital (HOMO) without altering the particle size. Outcomes of thermoelectric characterization was analyzed referring to the difference $\Delta E_{HOMO} = E_{HOMO}^{PEDOT:PSS} - E_{HOMO}^{CQD}$, with $-0.5\,eV \leq \Delta E_{HOMO} \leq +0.5\,eV$ [Fig. 11(b)].

The filtering process proposed by the authors is displayed in Fig. 11(a). Embedding CQDs into the insulating matrix enabled the formation of an additional path for the hopping transport of charge carriers, which can hop from PEDOT to PSS or to the CQDs depending on their energy states. The reduction of the energy gap [Fig. 11(a)] observed when $\Delta E_{HOMO} \leq 0$ allows hot holes to pass through the CQDs, while cold holes are blocked by the PSS insulating shell. Then, since hot holes exhibit higher mobility, a simultaneous enhancement of both S and σ is observed. The inclusion of CQDs also suppressed the thermal conductivity, leading to a zT of 0.32, a value comparable to that of inorganic thermoelectric materials.

Extrinsic energy filtering was also showcased in fully inorganic composites. Burkov and co-workers analyzed scattering at the interface between nanograins of semiconducting $CrSi_2$ diluted in an amorphous Cr–Si matrix,[89] which complements findings by Faleev and Leonard who reported EEF in metallic nanoinclusions embedded in a semiconducting host (PbTe).[90]

E. Extrinsic energy filtering in polymers

Transport in conducting polymers was reanalyzed by Kang and Snyder.[91] Their model allows a unified analysis of transport coefficients over a wide range electrical conductivity, using the spectral conductivity function $\sigma(E)$ that depends on the transport edge energy E_t,

$$\sigma(E) = \begin{cases} \sigma_{E_0}(T)\left(\frac{E - E_t}{k_B T}\right)^s & E > E_t, \\ 0 & E < E_t, \end{cases} \tag{10}$$

where E is charge carrier energy, $\sigma_{E_0}(T)$ is a transport coefficient, independent of the energy, and s is a transport exponent. Taking advantage of this model, Lin *et al.*[92] were able to identify and provide preliminary demonstration of EEF at organic/inorganic interface. In detail, they investigated the polyaniline/multiwalled carbon nanotube system (PANI/MWCNT). From an experimental perspective, carbon nanotubes synthesized through CVD were used as a template for polyaniline polymerization, with the PANI content varied from 0% to 30%.

The electrical conductivity of the hybrid composite decreases with increasing temperature but remains higher than that of pristine MWCNT at all temperatures. At the same time, the Seebeck coefficient of the PANI/MWCNT composites slightly increases with temperature, exceeding that of pure MWCNT only at room temperature. Figure 12(a) shows the $S - \sigma$ curves from 100 to 300 K. According to Eq. (10), the model is able to fit the experimental data with $s = 2$ up to 200 K, while for $T > 220$ K the model fits the data with $s = 3$. Thus, the change in the transport exponent was interpreted as an indication of a transition in the scattering mechanism at the PANI/MWCNT interface around 220 K. Moreover, Fig. 12(b) shows the band diagram of the PANI/MWCNT interface. Due to the difference in work functions, band banding occurs at the interface, forming a barrier of 90 meV, namely, of the proper height to filter out low-energy carriers.

F. Extrinsic energy filtering in intermetallics

Intermetallic compounds were investigated by Xia *et al.*[93] To explain the large negative Seebeck coefficient observed in CoSi, the authors employed the BTE under the relaxation-time approximation to compute the transport coefficients. By analyzing the band structure, they confirmed that a sudden change in the density of states near the

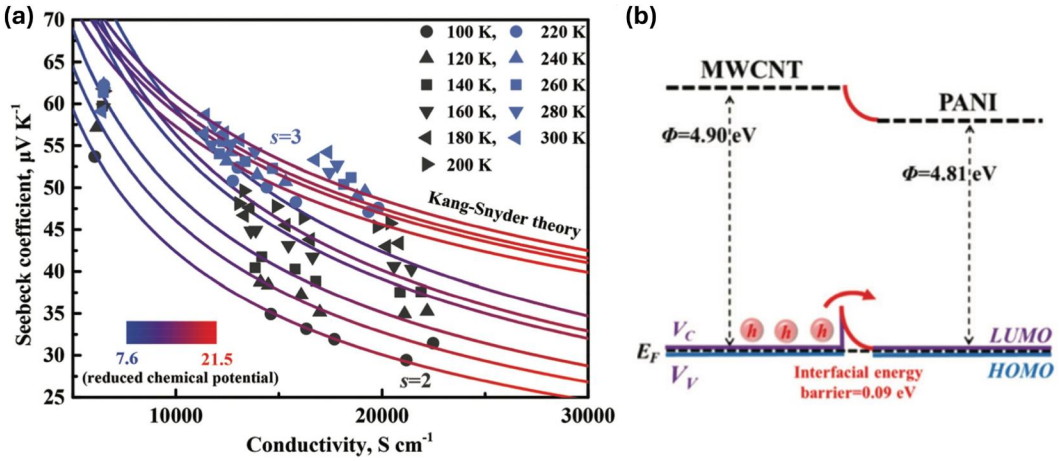

FIG. 12. (a) Kang–Snyder model (S vs σ) from 100 to 300 K. The different values of transport parameters required around 220 K mark a different scattering mechanism at the PANI/MWCNT interface. (b) Band alignment and filtering process at the PANI/MWCNT interface. Reprinted with permission from Lin *et al.*, Nanoscale **14**, 9419–9430 (2022). Copyright 2022 Royal Society of Chemistry.

05 May 2026 08:18:17

© Author(s) 2026

Fermi level induced preferential electron–phonon scattering, filtering out low-energy carriers, and thus enhancing the Seebeck coefficient.

VI. SUMMARY AND CONCLUSIONS

The experimental evidence reported in Sec. V is in agreement with the theoretical analyses presented in Sec. III, confirming the effectiveness of EEF in enhancing the thermoelectric properties of several materials, both bulk and thin films. We summarize here the three key questions we addressed in this review, namely, (1) why we should choose EEF to improve thermoelectric materials, (2) how EEF can be recognized, and (3) how it can be implemented in a thermoelectric material.

On the first count and as discussed in Secs. II and IV, EEF is not the only strategy available to obtain better thermoelectric materials. As of their performance, Gayner and Amouyal[94] compared the effects of several approaches—including hierarchical structures, band convergence, band engineering, and nanostructuring. Energy filtering exhibited the highest enhancement factor for both PF and zT compared to pristine material (2.9× and 4.6×, respectively). Another noteworthy aspect concerns thermal conductivity. The presence of second phases, potential barriers, impurities or nanoinclusions reduces the value of κ compared to the pristine material, consistent with the large enhancement of zT.

An enhancement of PF and zT is however not sufficient to claim EEF to be active in a given system. The presence of potential barriers is a necessary, yet not sufficient condition to activate EEF. As reported in Sec. IV, characterization techniques must be used to confirm and identify EEF. Some of these methods are complex and are not suitable for preliminary investigations. Therefore, EEF is best approached through two strategies, namely, preliminary and confirmatory analyses. Among the preliminary evidence, an increased Seebeck coefficient along with an unchanged, or even higher, electrical conductivity, is the most typical. This type of characterizations are simple and can be performed with a very simple and common setup. However, since a larger carrier mobility plays a key role in the EEF, the temperature dependent Hall effect measurement should be used as an additional preliminary analysis confirming the occurrence of EEF. If these preliminary characterizations suggest EEF to have arisen, more detailed analysis should be carried out. As discussed in Sec. IV, direct evidence of grain boundaries or of interfaces inducing potential barriers can be obtained by SEM and TEM. The nature of the potential barriers can be further elucidated by complementary techniques such as ARPES or Atomic Probe Tomography, which provides a space-resolved elemental map of the sample, confirming the presence of second phases that may cause interfacial potential barriers. In summary, the most reliable strategy to identify EEF is a rational, stepwise approach beginning with a theoretical study of the material followed by standard thermoelectric characterizations to obtain preliminary evidence of EEF. Confirmation requires instead more sophisticated analyses, which are however increasingly available and that should be deployed to sustain EEF claims.

Elements enabling the positive detection of EEF in thermoelectric materials also drive strategies to implement it. A proper, accurate design of the materials micro- or nanostructure is a first element to consider, as interfaces are the most common structural feature introducing potential barriers capable to filter out low-energy charge carriers. To this aim, as reported in Sec. V, one of the most common approaches to promote EEF involves the incorporation of nanoinclusions and secondary phases in matrix—and grain boundary engineering (e.g., by controlled precipitation of a second phase) as well. Along with it, another fundamental aspect of EEF implementation is theoretical modeling. As shown, computation of band structure and transport mechanism are an excellent guide to predict barrier height, which should not exceed $\approx 2k_BT$. Thus, overall, the implementation of EEF in a thermoelectric material requires a simultaneous theoretical and experimental effort—often followed by an extensive optimization, essential to maximize EEF effect and, finally, the performance of the material.

In summary, both intrinsic and extrinsic energy filtering are powerful and increasingly popular tools to enhance the power factor of thermoelectric materials. Although both lead to energy-selective carrier scattering, they apply to different classes of materials. Intrinsic energy filtering has been convincingly reported in gapless and metallic materials, while EEF is used to enhance PF in semiconductors. Excellent results have been achieved in both classes of materials. In metals, exploitation of IEF is strictly related to the materials' electronic structure, while EEF provides a tool to enhance the PF of many semiconductors through the introduction of barriers at GBs or at phase boundaries. As many other tools proposed and implemented over the last 20 years,[3] intrinsic and extrinsic EF effectively concur in the making of better thermoelectric materials and systems.

This said, in this review we have shown how care must be taken before claiming EEF to occur just based upon the simultaneous increase in the Seebeck coefficient and the electrical conductivity. Based on theoretical analyses, criteria to effectively sustain EEF as the mechanism responsible for the enhanced efficiency of thermoelectric materials have been presented and discussed. At the same time, such criteria also point out how materials can be tailored to activate EEF, mostly based on the control of the system nanostructure.

Although EEF rests nowadays on consistent and well established theoretical bases, further effort to extend its analysis to bulk materials where barrier spacing and height are statistically distributed is still needed. On the experimental side, relatively novel techniques such as Atomic Probe Tomography are expected to further strengthen EEF claims, also helping unravel the interplay between barrier height and grain boundary decoration, still a path to EEF activation not fully exploited.

ACKNOWLEDGMENTS

A.M. acknowledges the support received by the European Union—NextGenerationEU, Mission 4, Component 2.

AUTHOR DECLARATIONS

Conflict of Interest

The authors have no conflicts to disclose.

Author Contributions

A. Mazzacua: Conceptualization (supporting); Formal analysis (equal); Methodology (equal); Writing – original draft (lead); Writing – review & editing (equal). **F. Giulio:** Conceptualization (supporting); Formal analysis (equal); Methodology (supporting); Writing – review & editing (supporting). **D. Narducci:** Conceptualization (lead); Formal analysis (equal); Funding acquisition (lead); Methodology

05 May 2026 08:18:17

© Author(s) 2026

(equal); Project administration (lead); Supervision (lead); Validation (lead); Writing – original draft (supporting); Writing – review & editing (equal).

DATA AVAILABILITY

Data sharing is not applicable to this article as no new data were created or analyzed in this study.

REFERENCES

[1]D. Narducci, "Thermoelectric harvesters and the Internet of Things: Technological and economic drivers," J. Phys. Energy **1**, 024001 (2019).
[2]C. Goupil, *Continuum Theory and Modeling of Thermoelectric Elements* (Wiley, 2016).
[3]D. Beretta, N. Neophytou, J. M. Hodges, M. G. Kanatzidis, D. Narducci, M. Martin-Gonzalez, M. Beekman, B. Balke, G. Cerretti, W. Tremel *et al.*, "Thermoelectrics: From history, a window to the future," Mater. Sci. Eng., R **138**, 210–255 (2018).
[4]A. I. Hochbaum, R. K. Chen, R. D. Delgado, W. J. Liang, E. C. Garnett, M. Najarian, A. Majumdar, and P. D. Yang, "Enhanced thermoelectric performance of rough silicon nanowires," Nature **451**, 163–167 (2008).
[5]A. Boukai, Y. Bunimovich, J. Tahir-Kheli, J. Yu, W. Goddard, and J. Heath, "Silicon nanowires as efficient thermoelectric materials," Nature **451**, 168–171 (2008).
[6]L. D. Hicks and M. S. Dresselhaus, "Effect of quantum-well structures on the thermoelectric figure of merit," Phys. Rev. B **47**, 12727–12731 (1993).
[7]L. D. Hicks and M. S. Dresselhaus, "Thermoelectric figure of merit of a one-dimensional conductor," Phys. Rev. B **47**, 16631–16634 (1993).
[8]Y. Lan, A. J. Minnich, G. Chen, and Z. Ren, "Enhancement of thermoelectric figure-of-merit by a bulk nanostructuring approach," Adv. Funct. Mater. **20**, 357–376 (2010).
[9]M. Zebarjadi, G. Joshi, G. Zhu, B. Yu, A. Minnich, Y. Lan, X. Wang, M. Dresselhaus, Z. Ren, and G. Chen, "Power factor enhancement by modulation doping in bulk nanocomposites," Nano Lett. **11**, 2225–2230 (2011).
[10]D. Narducci, L. Zulian, B. Lorenzi, F. Giulio, and E. Villa, "Exceptional thermoelectric power factors in hyperdoped, fully dehydrogenated nanocrystalline silicon thin films," Appl. Phys. Lett. **119**, 263903 (2021).
[11]J. Mao, Z. Liu, and Z. Ren, "Size effect in thermoelectric materials," npj Quantum Mater. **1**, 1–9 (2016).
[12]J. P. Heremans, B. Wiendlocha, and A. M. Chamoire, "Resonant levels in bulk thermoelectric semiconductors," Energy Environ. Sci. **5**, 5510–5530 (2012).
[13]F. Garmroudi, S. Di Cataldo, M. Parzer, J. Coulter, Y. Iwasaki, M. Grasser, S. Stockinger, S. Pázmán, S. Witzmann, A. Riss *et al.*, "Energy filtering-induced ultrahigh thermoelectric power factors in Ni_3Ge," Sci. Adv. **11**, eadv7113 (2025).
[14]D. Narducci, E. Selezneva, G. Cerofolini, S. Frabboni, and G. Ottaviani, "Impact of energy filtering and carrier localization on the thermoelectric properties of granular semiconductors," J. Solid State Chem. **193**, 19–25 (2012).
[15]J. Y. Seto, "The electrical properties of polycrystalline silicon films," J. Appl. Phys. **46**, 5247–5254 (1975).
[16]A. Masci, E. Dimaggio, N. Neophytou, D. Narducci, and G. Pennelli, "Large increase of the thermoelectric power factor in multi-barrier nanodevices," Nano Energy **132**, 110391 (2024).
[17]F. Garmroudi, M. Parzer, A. Riss, C. Bourgès, S. Khmelevskyi, T. Mori, E. Bauer, and A. Pustogow, "High thermoelectric performance in metallic NiAu alloys via interband scattering," Sci. Adv. **9**, eadj1611 (2023).
[18]S. Thébaud, C. Adessi, and G. Bouzerar, "Large enhancement of the thermoelectric power factor in disordered materials through resonant scattering," Phys. Rev. B **99**, 245203 (2019).
[19]G. D. Mahan and J. O. Sofo, "The best thermoelectric," Proc. Natl. Acad. Sci. U. S. A. **93**, 7436–7439 (1996).
[20]J. P. Heremans, V. Jovovic, E. S. Toberer, A. Saramat, K. Kurosaki, A. Charoenphakdee, S. Yamanaka, and G. J. Snyder, "Enhancement of thermoelectric efficiency in PbTe by distortion of the electronic density of states," Science **321**, 554–557 (2008).
[21]P. Graziosi, K.-I. Mehnert, R. Dutt, J.-W. G. Bos, and N. Neophytou, "Materials design criteria for ultrahigh thermoelectric power factors in metals," PRX Energy **3**, 043009 (2024).
[22]D. M. Rowe and G. Min, "Multiple potential barriers as a possible mechanism to increase the Seebeck coefficient and electrical power factor," AIP Conf. Proc. **316**, 339–342 (1994).
[23]L. W. Whitlow and T. Hirano, "Superlattice applications to thermoelectricity," J. Appl. Phys. **78**, 5460–5466 (1995).
[24]Y. N. Y. Nishio and T. H. T. Hirano, "Improvement of the efficiency of thermoelectric energy conversion by utilizing potential barriers," Jpn. J. Appl. Phys. **36**, 170 (1997).
[25]H. Anno, T. Sakakibara, Y. Notohara, H. Tashiro, T. Koyanagi, H. Kaneko, and K. Matsubara, "Preparation and thermoelectric properties of $CoSb_3$ thin films on GaAs (100) substrate," in *XVI ICT'97. Proceedings ICT'97. 16th International Conference on Thermoelectrics (Cat. No. 97TH8291)* (IEEE, 1997), pp. 338–342.
[26]K. Kishimoto, M. Tsukamoto, and T. Koyanagi, "Temperature dependence of the Seebeck coefficient and the potential barrier scattering of n-type PbTe films prepared on heated glass substrates by RF sputtering," J. Appl. Phys. **92**, 5331–5339 (2002).
[27]D. Narducci, S. Frabboni, and X. Zianni, "Silicon de novo: Energy filtering and enhanced thermoelectric performances of nanocrystalline silicon and silicon alloys," J. Mater. Chem. C **3**, 12176–12185 (2015).
[28]D. Vashaee and A. Shakouri, "Improved thermoelectric power factor in metal-based superlattices," Phys. Rev. Lett. **92**, 106103 (2004).
[29]J. Zide, D. Vashaee, Z. Bian, G. Zeng, J. Bowers, A. Shakouri, and A. Gossard, "Demonstration of electron filtering to increase the Seebeck coefficient in $In_{0.53}Ga_{0.47}As/In_{0.53}Ga_{0.28}Al_{0.19}As$ superlattices," Phys. Rev. B **74**, 205335 (2006).
[30]M. Bachmann, M. Czerner, and C. Heiliger, "Ineffectiveness of energy filtering at grain boundaries for thermoelectric materials," Phys. Rev. B **86**, 115320 (2012).
[31]G. Green, "An essay on the application of mathematical analysis to the theories of electricity and magnetism," J. Reine Angew. Math. (Crelles J.) **1854**, 161–221 (2008), arXiv:0807.0088.
[32]Y. Kajikawa, "Conduction model covering non-degenerate through degenerate polycrystalline semiconductors with non-uniform grain-boundary potential heights based on an energy filtering model," J. Appl. Phys. **112**, 123713 (2012).
[33]Y. Kajikawa, "Effects of potential barrier height and its fluctuations at grain boundaries on thermoelectric properties of polycrystalline semiconductors," J. Appl. Phys. **114**, 053707 (2013).
[34]J.-H. Bahk, Z. Bian, and A. Shakouri, "Electron energy filtering by a nonplanar potential to enhance the thermoelectric power factor in bulk materials," Phys. Rev. B **87**, 075204 (2013).
[35]N. Neophytou and H. Kosina, "Optimizing thermoelectric power factor by means of a potential barrier," J. Appl. Phys. **114**, 044315 (2013).
[36]D. Narducci, E. Selezneva, G. Cerofolini, S. Frabboni, and G. Ottaviani, "High figures of merit in degenerate semiconductors. Energy filtering by grain boundaries in heavily doped polycrystalline silicon," AIP Conf. Proc. **1449**, 311–314 (2012).
[37]X. Zianni and D. Narducci, "Parametric modeling of energy filtering by energy barriers in thermoelectric nanocomposites," J. Appl. Phys. **117**, 035102 (2015).
[38]N. Neophytou, S. Foster, V. Vargiamidis, G. Pennelli, and D. Narducci, "Nanostructured potential well/barrier engineering for realizing unprecedentedly large thermoelectric power factors," Mater. Today Phys. **11**, 100159 (2019).
[39]P. Priyadarshi, V. Vargiamidis, and N. Neophytou, "Energy filtering in doping modulated nanoengineered thermoelectric materials: A Monte Carlo simulation approach," Materials **17**, 3522 (2024).
[40]R. Kim and M. S. Lundstrom, "Computational study of energy filtering effects in one-dimensional composite nano-structures," J. Appl. Phys. **111**, 024508 (2012).
[41]N. Neophytou and M. Thesberg, "Modulation doping and energy filtering as effective ways to improve the thermoelectric power factor," J. Comput. Electron. **15**, 16–26 (2016).
[42]D. Narducci, B. Lorenzi, X. Zianni, N. Neophytou, S. Frabboni, G. C. Gazzadi, A. Roncaglia, and F. Suriano, "Enhancement of the power factor in two-phase

05 May 2026 08:18:17

© Author(s) 2026

silicon–boron nanocrystalline alloys," Phys. Status Solidi A **211**, 1255–1258 (2014).
[43]H. Sang, W. Wang, Z. Wang, M. Hong, C. Zhang, S. Xie, H. Ge, F. Yan, Z. Wang, Y. Ouyang *et al.*, "Tailoring interfacial charge transfer for optimizing thermoelectric performances of MnTe-Sb_2Te_3 superlattice-like films," Adv. Funct. Mater. **33**, 2210213 (2023).
[44]A. Soni, Y. Shen, M. Yin, Y. Zhao, L. Yu, X. Hu, Z. Dong, K. A. Khor, M. S. Dresselhaus, and Q. Xiong, "Interface driven energy filtering of thermoelectric power in spark plasma sintered $Bi_2Te_{2.7}Se_{0.3}$ nanoplatelet composites," Nano Lett. **12**, 4305–4310 (2012).
[45]A. Soni, Z. Yanyuan, Y. Ligen, M. K. K. Aik, M. S. Dresselhaus, and Q. Xiong, "Enhanced thermoelectric properties of solution grown $Bi_2Te_{3-x}Se_x$ nanoplatelet composites," Nano Lett. **12**, 1203–1209 (2012).
[46]Y. Zhong, J. Tang, H. Liu, Z. Chen, L. Lin, D. Ren, B. Liu, and R. Ang, "Optimized strategies for advancing n-type PbTe thermoelectrics: A review," ACS Appl. Mater. Interfaces **12**, 49323–49334 (2020).
[47]Y. Kawajiri, S.-A. Tanusilp, M. Kumagai, M. Ishimaru, Y. Ohishi, J. Tanaka, and K. Kurosaki, "Enhancement of thermoelectric properties of n-type $Bi_2Te_{3-x}Se$ by energy filtering effect," ACS Appl. Energy Mater. **4**, 11819–11826 (2021).
[48]J. Zhang, D. Wu, D. He, D. Feng, M. Yin, X. Qin, and J. He, "Extraordinary thermoelectric performance realized in n-type PbTe through multiphase nanostructure engineering," Adv. Mater. **29**, 1703148 (2017).
[49]H.-T. Liu, Q. Sun, Y. Zhong, Q. Deng, L. Gan, F.-L. Lv, X.-L. Shi, Z.-G. Chen, and R. Ang, "High-performance in n-type PbTe-based thermoelectric materials achieved by synergistically dynamic doping and energy filtering," Nano Energy **91**, 106706 (2022).
[50]H. Yang, J.-H. Bahk, T. Day, A. M. Mohammed, G. J. Snyder, A. Shakouri, and Y. Wu, "Enhanced thermoelectric properties in bulk nanowire heterostructure-based nanocomposites through minority carrier blocking," Nano Lett. **15**, 1349–1355 (2015).
[51]H. Cho, S. Y. Back, J. H. Yun, S. Byeon, H. Jin, and J.-S. Rhyee, "Thermoelectric properties and low-energy carrier filtering by Mo microparticle dispersion in an n-type $CuI_{0.003}Bi_2(Te,Se)_3$ bulk matrix," ACS Appl. Mater. Interfaces **12**, 38076–38084 (2020).
[52]A. Pakdel, Q. Guo, V. Nicolosi, and T. Mori, "Enhanced thermoelectric performance of Bi-Sb-Te/Sb_2O_3 nanocomposites by energy filtering effect," J. Mater. Chem. A **6**, 21341–21349 (2018).
[53]D. Liu, D. Wang, T. Hong, Z. Wang, Y. Wang, Y. Qin, L. Su, T. Yang, X. Gao, Z. Ge *et al.*, "Lattice plainification advances highly effective SnSe crystalline thermoelectrics," Science **380**, 841–846 (2023).
[54]Y. Lu, Y. Qiu, K. Cai, Y. Ding, M. Wang, C. Jiang, Q. Yao, C. Huang, L. Chen, and J. He, "Ultrahigh power factor and flexible silver selenide-based composite film for thermoelectric devices," Energy Environ. Sci. **13**, 1240–1249 (2020).
[55]R. Xu, L. Huang, J. Zhang, D. Li, J. Liu, J. Liu, J. Fang, M. Wang, and G. Tang, "Nanostructured SnSe integrated with Se quantum dots with ultrahigh power factor and thermoelectric performance from magnetic field-assisted hydrothermal synthesis," J. Mater. Chem. A **7**, 15757–15765 (2019).
[56]Z. Ma, C. Wang, J. Lei, D. Zhang, Y. Chen, Y. Wang, J. Wang, and Z. Cheng, "Core–shell nanostructures introduce multiple potential barriers to enhance energy filtering for the improvement of the thermoelectric properties of SnTe," Nanoscale **12**, 1904–1911 (2020).
[57]F. Ahmed, N. Tsujii, and T. Mori, "Thermoelectric properties of $CuGa_{1-x}Mn_xTe_2$: Power factor enhancement by incorporation of magnetic ions," J. Mater. Chem. A **5**, 7545–7554 (2017).
[58]J. Tang, R. Xu, J. Zhang, D. Li, W. Zhou, X. Li, Z. Wang, F. Xu, G. Tang, and G. Chen, "Light element doping and introducing spin entropy: An effective strategy for enhancement of thermoelectric properties in BiCuSeO," ACS Appl. Mater. Interfaces **11**, 15543–15551 (2019).
[59]W. Yan, X. Nie, S. Ke, Y. Hu, X. Ai, W. Zhu, W. Zhao, and Q. Zhang, "Magnetic-anisotropy-enhanced electrical transport properties of Co/$Bi_{0.5}Sb_{1.5}Te_3$/PVDF flexible thermoelectromagnetic films," Adv. Funct. Mater. **32**, 2209739 (2022).
[60]B. Zhou, S. Li, W. Li, J. Li, X. Zhang, S. Lin, Z. Chen, and Y. Pei, "Thermoelectric properties of SnS with Na-doping," ACS Appl. Mater. Interfaces **9**, 34033–34041 (2017).
[61]J. Heo, G. Laurita, S. Muir, M. A. Subramanian, and D. A. Keszler, "Enhanced thermoelectric performance of synthetic tetrahedrites," Chem. Mater. **26**, 2047–2051 (2014).
[62]A. V. Powell, "Recent developments in earth-abundant copper-sulfide thermoelectric materials," J. Appl. Phys. **126**, 100901 (2019).
[63]B. Jiang, X. Liu, Q. Wang, J. Cui, B. Jia, Y. Zhu, J. Feng, Y. Qiu, M. Gu, Z. Ge *et al.*, "Realizing high-efficiency power generation in low-cost PbS-based thermoelectric materials," Energy Environ. Sci. **13**, 579–591 (2020).
[64]J. Mani, S. Radha, F. J. Prita, R. Rajkumar, M. Arivanandhan, and G. Anbalagan, "Enhancing the thermoelectric performance of Cu_2S/CuO nanocomposites through energy-filtering effect and phonon scattering," J. Inorg. Organomet. Polym. Mater. **34**, 1548–1563 (2024).
[65]X.-Q. Chen, S.-J. Fan, C. Han, T. Wu, L.-J. Wang, W. Jiang, W. Dai, and J.-P. Yang, "Multiscale architectures boosting thermoelectric performance of copper sulfide compound," Rare Met. **40**, 2017–2025 (2021).
[66]S. Luo, J. Liang, Z. Wei, Y. Du, L. Lv, Y. Jiang, S. Zheng, W. Song, and Z. Zhang, "Simultaneously boosting electrical and thermal transport properties of $CuGaTe_2$ through XCl_2 (X = Cd, Zn) doping-driven band and defect engineering," J. Mater. Chem. A **13**, 4380–4389 (2025).
[67]B. Lorenzi, D. Narducci, R. Tonini, S. Frabboni, G. C. Gazzadi, G. Ottaviani, N. Neophytou, and X. Zianni, "Paradoxical enhancement of the power factor of polycrystalline silicon as a result of the formation of nanovoids," J. Electron. Mater. **43**, 3812–3816 (2014).
[68]G. Ren, J. Lan, C. Zeng, Y. Liu, B. Zhan, S. Butt, Y.-H. Lin, and C.-W. Nan, "High performance oxides-based thermoelectric materials," JOM **67**, 211–221 (2015).
[69]W. Shin and N. Murayama, "High performance p-type thermoelectric oxide based on NiO," Mater. Lett. **45**, 302–306 (2000).
[70]P. Mele, S. Saini, A. Tiwari, P. Hopkins, K. Miyazaki, A. Ichinose, J. Niemelä, and M. Karppinen, "Thermoelectric and structural characterization of Al-doped ZnO/Y_2O_3 multilayers," J. Nanosci. Nanotechnol. **17**, 1616–1621 (2017).
[71]J. Linnera, G. Sansone, L. Maschio, and A. J. Karttunen, "Thermoelectric properties of p-type Cu_2O, CuO, and NiO from hybrid density functional theory," J. Phys. Chem. C **122**, 15180–15189 (2018).
[72]D. Bérardan, E. Guilmeau, A. Maignan, and B. Raveau, "In_2O_3:Ge, a promising n-type thermoelectric oxide composite," Solid State Commun. **146**, 97–101 (2008).
[73]K. Kurosaki, H. Muta, M. Uno, and S. Yamanaka, "Thermoelectric properties of $NaCo_2O_4$," J. Alloys Compd. **315**, 234–236 (2001).
[74]C. Gayner, Y. Natanzon, and Y. Amouyal, "Effects of co-doping and microstructure on charge carrier energy filtering in thermoelectric titanium-doped zinc aluminum oxide," ACS Appl. Mater. Interfaces **14**, 4035–4050 (2022).
[75]D. Narducci and F. Giulio, "Recent advances on thermoelectric silicon for low-temperature applications," Materials **15**, 1214 (2022).
[76]C. B. Vining, "The thermoelectric properties of boron-doped silicon and silicon-germanium in the as-hot pressed conditions," Technical Report (Jet Propulsion Laboratory/California Institute of Technology, 1988).
[77]C. B. Vining, W. Laskow, J. O. Hanson, R. R. Van der Beck, and P. D. Gorsuch, "Thermoelectric properties of pressure–sintered $Si_{0.8}Ge_{0.2}$ thermoelectric alloys," J. Appl. Phys. **69**, 4333–4340 (1991).
[78]S. Loughin, D. X. Centurioni, A. G. Robison, J. J. Maley, and J. P. Fleurial, "High-boron p-type silicon germanium thermoelectric material prepared by the vacuum casting and hot pressing method," AIP Conf. Proc. **271**, 747–752 (1993).
[79]G. Joshi, H. Lee, Y. Lan, X. Wang, G. Zhu, D. Wang, R. W. Gould, D. C. Cuff, M. Y. Tang, M. S. Dresselhaus, G. Chen, and Z. Ren, "Enhanced thermoelectric figure-of-merit in nanostructured p-type silicon germanium bulk alloys," Nano Lett. **8**, 4670–4674 (2008).
[80]X. W. Wang, H. Lee, Y. C. Lan, G. H. Zhu, G. Joshi, D. Z. Wang, J. Yang, A. J. Muto, M. Y. Tang, J. Klatsky, S. Song, M. S. Dresselhaus, G. Chen, and Z. F. Ren, "Enhanced thermoelectric figure of merit in nanostructured n-type silicon germanium bulk alloy," Appl. Phys. Lett. **93**, 193121 (2008).
[81]D. Narducci, E. Selezneva, A. Arcari, G. Cerofolini, E. Romano, R. Tonini, and G. Ottaviani, "Enhanced thermoelectric properties of strongly degenerate polycrystalline silicon upon second phase segregation," in *MRS Online Proceedings Library (OPL)* (Springer, 2011), Vol. 1314.

05 May 2026 08:18:17

© Author(s) 2026

[82]N. Neophytou, X. Zianni, H. Kosina, S. Frabboni, B. Lorenzi, and D. Narducci, "Simultaneous increase in electrical conductivity and Seebeck coefficient in highly boron-doped nanocrystalline Si," Nanotechnology **24**, 205402 (2013).
[83]N. S. Bennett, D. Byrne, A. Cowley, and N. Neophytou, "Dislocation loops as a mechanism for thermoelectric power factor enhancement in silicon nanolayers," Appl. Phys. Lett. **109**, 173905 (2016).
[84]H. Jin, J. Li, J. Iocozzia, X. Zeng, P.-C. Wei, C. Yang, N. Li, Z. Liu, J. H. He, T. Zhu *et al.*, "Hybrid organic–inorganic thermoelectric materials and devices," Angew. Chem., Int. Ed. **58**, 15206–15226 (2019).
[85]M. Lindorf, K. Mazzio, J. Pflaum, K. Nielsch, W. Brütting, and M. Albrecht, "Organic-based thermoelectrics," J. Mater. Chem. A **8**, 7495–7507 (2020).
[86]X. Guan and J. Ouyang, "Enhancement of the Seebeck coefficient of organic thermoelectric materials via energy filtering of charge carriers," CCS Chem. **3**, 2415–2427 (2021).
[87]Z. Liang, M. J. Boland, K. Butrouna, D. R. Strachan, and K. R. Graham, "Increased power factors of organic–inorganic nanocomposite thermoelectric materials and the role of energy filtering," J. Mater. Chem. A **5**, 15891–15900 (2017).
[88]D. Kim, Y. Park, D. Ju, G. Lee, W. Kwon, and K. Cho, "Energy-filtered acceleration of charge-carrier transport in organic thermoelectric nanocomposites," Chem. Mater. **33**, 4853–4862 (2021).
[89]A. Burkov, S. Novikov, V. Khovaylo, and J. Schumann, "Energy filtering enhancement of thermoelectric performance of nanocrystalline Cr_{1-x} six composites," J. Alloys Compd. **691**, 89–94 (2017).
[90]S. V. Faleev and F. Léonard, "Theory of enhancement of thermoelectric properties of materials with nanoinclusions," Phys. Rev. B **77**, 214304 (2008).
[91]S. D. Kang and G. J. Snyder, "Charge-transport model for conducting polymers," Nat. Mater. **16**, 252–257 (2017).
[92]Z. Lin, H. Dang, C. Zhao, Y. Du, C. Chi, W. Ma, Y. Li, and X. Zhang, "The cross-interface energy-filtering effect at organic/inorganic interfaces balances the trade-off between thermopower and conductivity," Nanoscale **14**, 9419–9430 (2022).
[93]Y. Xia, J. Park, F. Zhou, and V. Ozoliņš, "High thermoelectric power factor in intermetallic CoSi arising from energy filtering of electrons by phonon scattering," Phys. Rev. Appl. **11**, 024017 (2019).
[94]C. Gayner and Y. Amouyal, "Energy filtering of charge carriers: Current trends, challenges, and prospects for thermoelectric materials," Adv. Funct. Mater. **30**, 1901789 (2020).

05 May 2026 08:18:17

© Author(s) 2026